Cell

Article

Enteric neuronal Piezo1 maintains mechanical and immunological homeostasis by sensing force

Graphical abstract

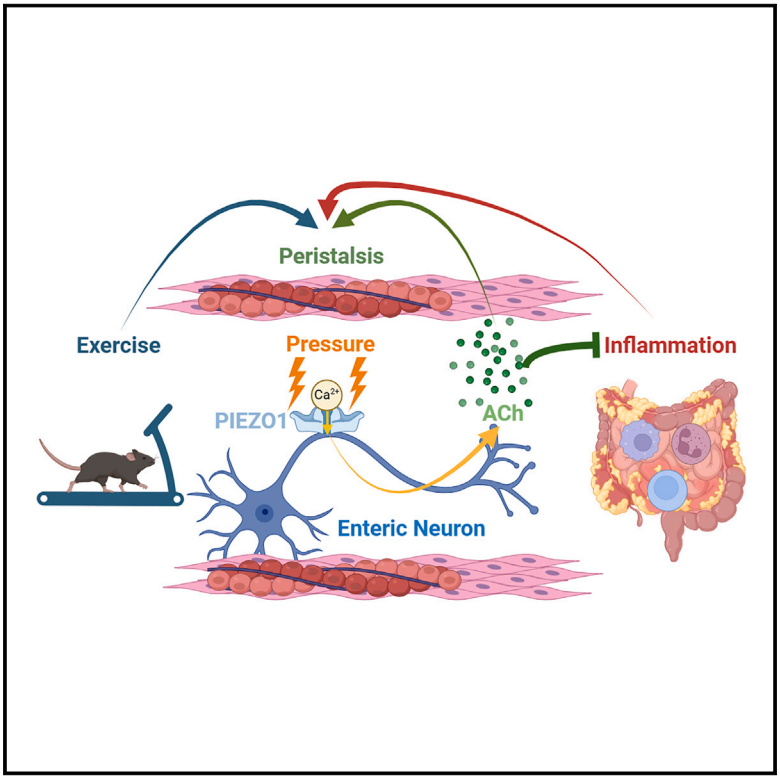

Highlights

- The enteric nervous system directly senses mechanical force via Piezo1
- Cholinergic enteric neurons functionally express the Piezo1 mechanosensor
- Piezo1 on cholinergic neurons is required to accelerate GI motility in response to force
- Cholinergic neuronal Piezo1-mechanosensation limits aberrant intestinal inflammation

Authors

Zili Xie, Lillian Rose, Jing Feng, ..., Nick J. Spencer, Hongzhen Hu, Ruaidhrí Jackson

Correspondence

hongzhen.hu@mssm.edu (H.H.), ruaidhri_jackson@hms.harvard.edu (R.J.)

In brief

Expression and functional analysis define how Piezo1-dependent cholinergic responses by enteric neurons directly sense luminal pressure to orchestrate digestion and inflammation in mice.

Xie et al., 2025, Cell *188*, 2417–2432
May 1, 2025
https://doi.org/10.1016/j.cell.2025.02.031

CellPress

Cell

CellPress

Article

Enteric neuronal Piezo1 maintains mechanical and immunological homeostasis by sensing force

Zili Xie,[1,2,11] Lillian Rose,[3,11] Jing Feng,[2,4] Yonghui Zhao,[2] Yisi Lu,[3] Harry Kane,[3] Timothy J. Hibberd,[5] Xueming Hu,[1,2] Zhen Wang,[1] Kaikai Zang,[2] Xingliang Yang,[1,2] Quentin Richardson,[3] Rahmeh Othman,[3] Olivia Venezia,[3] Ademi Zhakyp,[3] Fang Gao,[1,2] Nobuya Abe,[1] Keren Vigeland,[3] Hongshen Wang,[3] Camren Branch,[3] Coco Duizer,[3] Liwen Deng,[3] Xia Meng,[1] Lydia Zamidar,[1] Max Hauptschein,[3] Ronan Bergin,[6] Xinzhong Dong,[7] Issac M. Chiu,[3] Brian S. Kim,[1,8,9] Nick J. Spencer,[5] Hongzhen Hu,[1,2,8,9,10,12,*] and Ruaidhrí Jackson[3,12,13,*]

[1]Department of Dermatology, The Mark Lebwohl Center for Neuroinflammation and Sensation, Icahn School of Medicine at Mount Sinai, New York, NY 10019, USA

[2]Department of Anesthesiology, The Center for the Study of Itch & Sensory Disorders, Washington University School of Medicine, St. Louis, MO 63130, USA

[3]Department of Immunology, Harvard Medical School, Boston, MA 02115, USA

[4]Center for Neurological and Psychiatric Research and Drug Discovery, Shanghai Institute of Materia Medica, Chinese Academy of Science, University of Chinese Academy of Sciences, Beijing, China

[5]Visceral Neurophysiology Laboratory, College of Medicine and Public Health, Flinders University, Adelaide, SA, Australia

[6]Kathleen Lonsdale Institute for Human Health Research, Maynooth University, Maynooth, Ireland

[7]The Solomon H. Snyder Department of Neuroscience, Howard Hughes Medical Institute, Johns Hopkins University School of Medicine, Baltimore, MD 21205, USA

[8]Friedman Brain Institute, Icahn School of Medicine at Mount Sinai, New York, NY 10029, USA

[9]Allen Discovery Center for Neuroimmune Interactions, New York, NY 10029, USA

[10]The Nash Family Department of Neuroscience, Icahn School of Medicine at Mount Sinai, New York, NY 10029, USA

[11]These authors contributed equally

[12]Senior author

[13]Lead contact

*Correspondence: hongzhen.hu@mssm.edu (H.H.), ruaidhri_jackson@hms.harvard.edu (R.J.)

https://doi.org/10.1016/j.cell.2025.02.031

SUMMARY

The gastrointestinal (GI) tract experiences a myriad of mechanical forces while orchestrating digestion and barrier immunity. A central conductor of these processes, the enteric nervous system (ENS), detects luminal pressure to regulate peristalsis independently of extrinsic input from the central and peripheral nervous systems. However, how the ~500 million enteric neurons that reside in the GI tract sense and respond to force remains unknown. Herein, we establish that the mechanosensor *Piezo1* is functionally expressed in cholinergic enteric neurons. Optogenetic stimulation of Piezo1$^+$ cholinergic enteric neurons drives colonic motility, while Piezo1 deficiency reduces cholinergic neuronal activity and slows peristalsis. Additionally, Piezo1 deficiency in cholinergic enteric neurons abolishes exercise-induced acceleration of GI motility. Finally, we uncover that enteric neuronal Piezo1 function is required for motility alterations in colitis and acts to prevent aberrant inflammation and tissue damage. This work uncovers how the ENS senses and responds to mechanical force.

INTRODUCTION

The gastrointestinal (GI) tract is one of the most mechanically diverse environments in the body. Recently, mechanotransduction, or the process in which cells can convert physical forces into biochemical and electrochemical signals, has gained an increasing appreciation for its critical importance in regulating both digestive and immunological processes.[1–4] Despite the progress that has been made in the past few decades in unraveling the structure and function of the enteric nervous system (ENS), which is central to coordinating colonic motility and is a critical arbitrator of intestinal inflammation,[5–8] the molecules, cell types, and neural circuits that govern the process of mechanosensitivity in the ENS remain to be elucidated.

The greatest source of luminal forces in the large intestine arises from colonic migrating motor complexes (CMMCs), which have been identified as a major motor pattern regulating the movement of fecal matter along the colon and are known to be highly dependent on mechanical inputs.[9] CMMCs are disrupted in many disease conditions involving dysmotility, including slow-transit constipation and inflammatory bowel disease (IBD).[10,11] Therefore, by gaining a better understanding of how

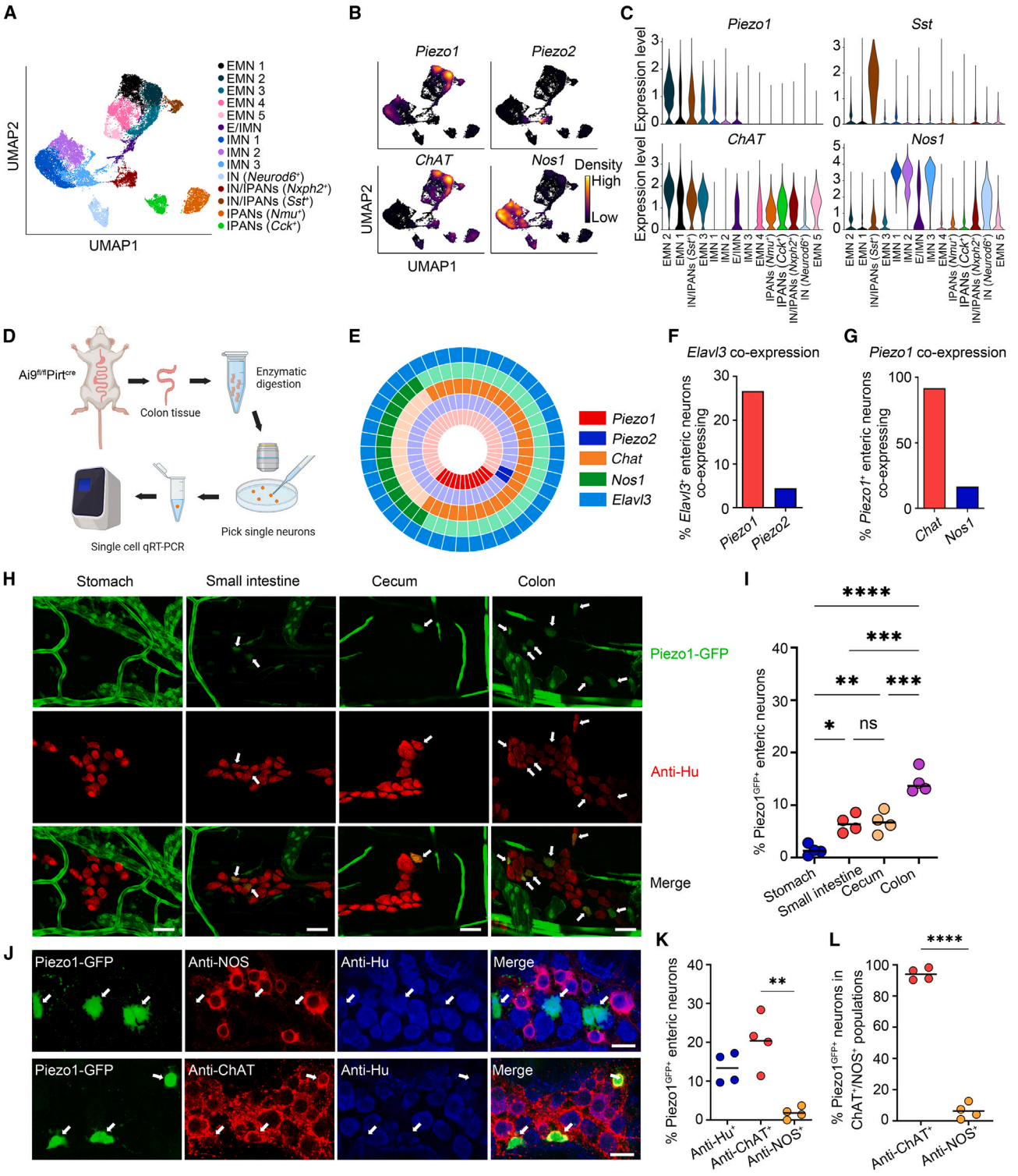

Figure 1. Piezo1 is specifically expressed in cholinergic enteric neurons

(A) Uniform manifold approximation and projection (UMAP) analysis of scRNA-seq integrated from 3 ENS datasets,[25–27] showing EMN, excitatory motor neuron; IMN, inhibitory motor neuron; IN, interneuron; IPANs, intrinsic primary afferent neurons.

(B) UMAP analysis of *Piezo1*, *Piezo2*, *Chat*, and nitric oxide synthase 1 (*Nos1)* gene expression in ENS population clusters depicted in (A).

(C) Violin plot analysis shows expression of *Piezo1*, *Sst*, *Chat*, and *Nos1.*

(D) Flowchart depicting the experimental procedure of single-cell real-time RT-qPCR.

(legend continued on next page)

mechanical processes are regulated and sensed, we may uncover much-needed therapeutic intervention strategies for these debilitating illnesses. While extrinsic somatosensory neurons[12,13] and autonomic nervous system projections regulate GI motility,[14–16] neuronal circuits inside the ENS can autonomously coordinate gut movements.[17,18] However, the intrinsic mechanosensitive elements in the intestine remain unidentified.

Consistent with the high dependence of CMMCs on mechenical inputs,[19] multiple GI cell types express mechanoreceptor Piezo family proteins.[20,21] Recently, it has been uncovered that the Piezo2 ion channels convert mechanical forces into the release of serotonin (5-HT) from the enterochromaffin cells (ECs) in the epithelium, enabling the GI tract to sense luminal forces in the intestine.[21] Furthermore, new studies have identified Piezo2 as molecular sensors in extrinsic GI innervating sensory neurons that function to slow GI transit.[12] However, the archetypal member of the Piezo family, Piezo1, in enteric neural circuits has no known role in digestion in mammals.[22–24]

Here, we identify that cholinergic enteric neurons express Piezo1 to sense pressure and regulate neuronal activity. Optogenetic stimulation or chemogenetic inhibition of Piezo1-expressing cholinergic neurons results in accelerated or retarded GI motility, respectively. Loss of Piezo1 in enteric cholinergic neurons prevents recognition of rising luminal intestinal pressure and disrupts GI motility. Finally, we demonstrate the necessity of intrinsic enteric neuronal Piezo1 in regulating exercise-induced GI motility acceleration and preventing intestinal inflammation in models of IBD. Our findings uncover how the ENS directly senses mechanical force in the intestine.

RESULTS

Cholinergic enteric neurons respond to mechanical force via Piezo1

To investigate the expression profiles of mechanosensitive Piezo ion channels in the ENS, we integrated 3 publicly available single-cell RNA sequencing (scRNA-seq) datasets of murine enteric neurons[25–27] (Figures 1A and S1A; Table S1). Interestingly, while *Piezo2* showed only limited expression in a subset of interneurons/intrinsic primary afferent neurons (IPANs), *Piezo1* was highly expressed in several cholinergic clusters identified by choline acetyltransferase$^+$ (ChAT$^+$), including over 50% of all excitatory motor neurons (Figures 1B, 1C, S1B, and S1C). Furthermore, by mining a human enteric neuron dataset,[25] we uncovered that *PIEZO1* was also expressed by human cholinergic neurons (Figures S1D and S1E).

Next, we conducted single-cell reverse transcriptase real-time quantitative PCR (real-time RT-qPCR) on enzymatically isolated individual tdTomato$^+$ enteric neurons from Ai9$^{fl/fl}$Pirt^{cre} mice (Figure 1D). We identified *Piezo1* expression in approximately 26.7% of all enteric neurons, with more than 91.7% of Piezo1$^+$ enteric neurons being cholinergic (Figures 1E–1G). To validate the expression of Piezo1 in the ENS *in situ*, we generated Piezo1^{flpo} mice that express flpo recombinase in Piezo1$^+$ cells (Figure S1F). By crossing to flpo-dependent GFP reporter mice, we detected Piezo1-driven GFP expression in several cell types in the mouse colon (Figures 1H and S1G). Enteric neuronal Piezo1-driven GFP was not observed in the stomach but was expressed in the small intestine, cecum, and the colon (Figures 1H and 1I) where it was mainly expressed in cholinergic myenteric neurons and was rarely expressed in nitrergic myenteric neurons (Figures 1J–1L, S1H, and S1I). Piezo1 was expressed in about 15% of all enteric neurons (identified by the anti-Hu$^+$ enteric neuronal cell body marker) and >20% of all cholinergic neurons in the colon (Figure 1K). Nearly all identified Piezo1$^+$ neurons co-expressed ChAT (Figures 1L and S1I). We additionally confirmed that PIEZO1 protein was expressed in myenteric cholinergic neurons of the Piezo1^{tdTomato} fusion protein reporter mouse strain[28] (Figures S1J and S1K). Furthermore, we uncovered that PIEZO1 localized to neuron projections in the mucosa (Figure S1L).

To uncover whether *Piezo1* is functionally expressed in enteric neurons, we first took a reductionist approach using cultured myenteric neurons from adult mice. Myenteric neuron cultures displayed a high level of *Piezo1* expression compared with *Piezo2* and other putative mechanosensory ion channels (Figure S2A). We stimulated enteric neuron cultures with the Piezo1 agonist Yoda1 and observed robust nuclear c-FOS accumulation compared with controls (Figures S2B and S2C), indicating Piezo1 stimulation results in neuronal activation.[29–31] Next, to uncover whether enteric neurons could respond to mechanical force, we subjected myenteric neuronal cultures to static and cyclical hydrostatic pressure (Figure S2D), as previously described.[4] Cyclical hydrostatic pressure resulted in a significant increase in the abundance of c-FOS nuclear localization (Figures S2E and S2F). Moreover, Yoda1 stimulation triggered

(E) Donut plot depicting the co-expression patterns of *Piezo1*, *Piezo2*, *Chat*, *Nos1*, and *Elavl3* in 45 Pirt-tdTomato$^+$ enteric neurons. Each gene is represented by a distinct color, with its expression highlighted by bold shading.
(F) Summary data from single-cell real-time RT-qPCR analysis of Pirt^{cre}-tdTomato$^+$ enteric neurons showing the percentage of enteric neurons expressing *Piezo1* and *Piezo2* in the *Elavl3*$^+$ population.
(G) Summary data from single-cell real-time RT-qPCR analysis of Pirt^{cre}-tdTomato$^+$ enteric neurons showing the percentage of Piezo1$^+$ enteric neurons that co-express *Chat* and *Nos1*.
(H) Immunofluorescence images of Piezo1-GFP$^+$ enteric neurons, co-stained with anti-GFP and anti-Hu, in whole-mount myenteric plexus preparations from the stomach, small intestine, cecum, and colon of Piezo1^{flpo}-GFP reporter mice. Scale bar: 40 μm.
(I) Summary data showing the percentage of Piezo1$^+$ enteric neurons among the total enteric neurons in the stomach, small intestine, cecum, and colon.
(J) Immunofluorescence images of Piezo1-GFP$^+$ enteric neurons, co-stained with anti-GFP, anti-NOS, anti-ChAT, and anti-Hu, in colonic enteric neurons of Piezo1^{flpo}GFP reporter mice. Scale bar: 25 μm.
(K) Summary data showing the percentage of Piezo1$^+$ enteric neurons among the total, ChAT$^+$, and NOS$^+$ ENS populations.
(L) Summary data showing the percentage of ChAT$^+$ and NOS$^+$ enteric neurons among the Piezo1$^+$ ENS population.
Statistics determined by two-tailed Student's t test. ns, no significant difference, $^*p < 0.05$, $^{**}p < 0.01$, $^{***}p < 0.001$, $^{****}p < 0.0001$.
See also Figure S1.

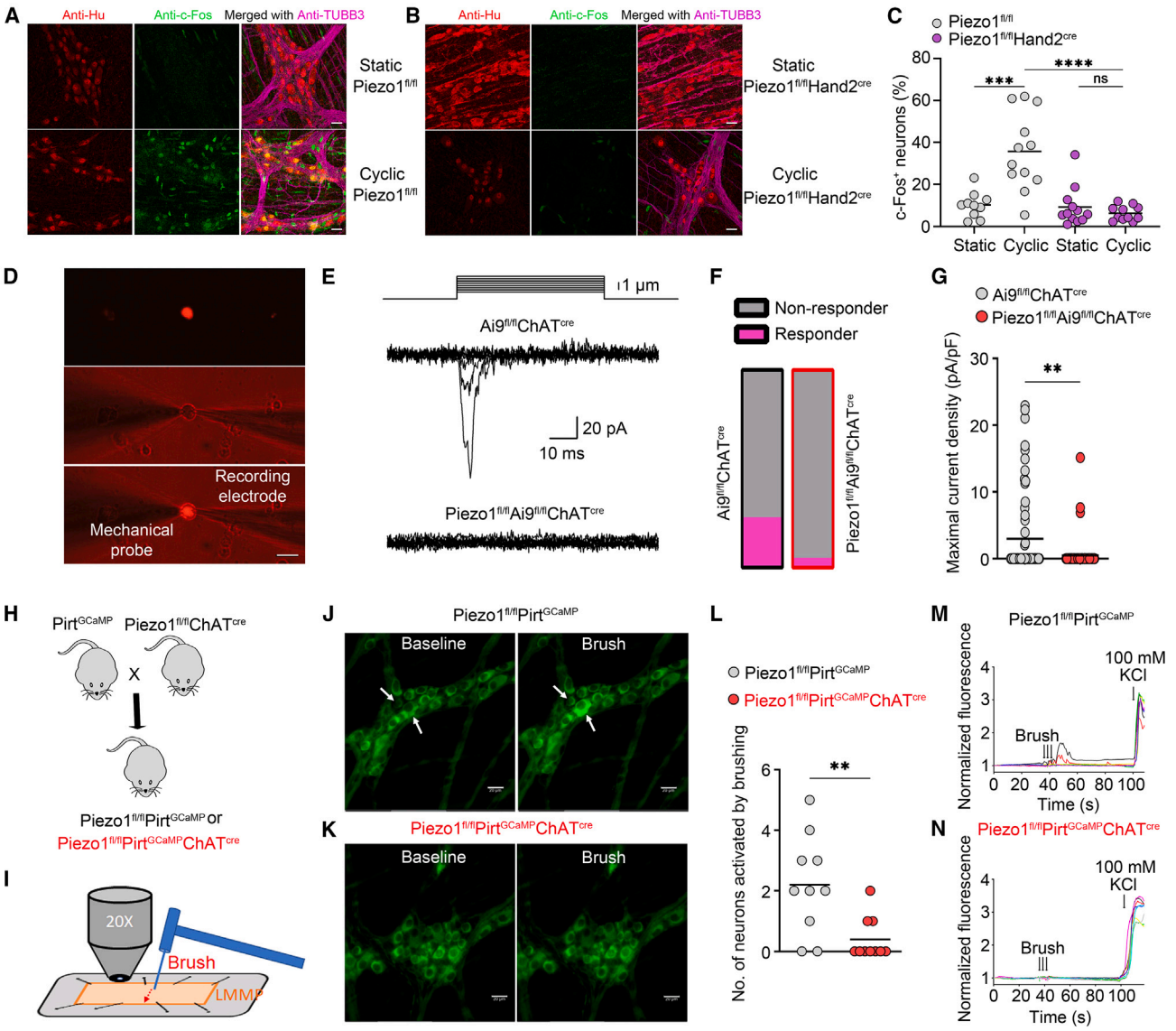

Figure 2. Cholinergic enteric neurons respond to mechanical force via Piezo1

(A) Immunofluorescence images of isolated colonic myenteric plexus stimulated with static or cyclic hydrostatic pressure, stained for anti-Hu, anti-c-Fos and anti-beta tubulin. Scale bar: 78 μm.

(B) Immunofluorescence images of isolated colonic myenteric plexus stimulated with static or cyclic hydrostatic pressure, stained for anti-Hu anti-c-Fos and anti-beta tubulin Scale bar: 78 μm.

(C) Quantification of the ratio of c-Fos^{+} neuron cell bodies to total neuron cell bodies stained in (A) and (B).

(D) Images illustrate the placement of a recording electrode and mechanical probe for the simultaneous recording of membrane current and mechanical stimulation on a tdTomato^{+} myenteric neuron isolated from an Ai9$^{fl/fl}$ChAT^{cre} mouse. Scale bar: 20 μm.

(E) Representative mechanically activated whole-cell currents, evoked by membrane displacements, were recorded in myenteric neurons isolated from Ai9$^{fl/fl}$ChAT^{cre} and Piezo1$^{fl/fl}$Ai9$^{fl/fl}$ChAT^{cre} mice.

(F) Summary data illustrating the frequency distribution of enteric neurons isolated from Ai9$^{fl/fl}$ChAT^{cre} and Piezo1$^{fl/fl}$Ai9$^{fl/fl}$ChAT^{cre} mice, characterized by the presence (responder) or absence (non-responder) of mechanically activated currents.

(G) Maximal current density of inward whole-cell mechanically activated currents in enteric neurons isolated from Ai9$^{fl/fl}$ChAT^{cre} and Piezo1$^{fl/fl}$Ai9$^{fl/fl}$ChAT^{cre} mice. n = 67 cells from 5 mice for Ai9$^{fl/fl}$ChAT^{cre} and n = 62 cells from 5 mice for Piezo1$^{fl/fl}$Ai9$^{fl/fl}$ChAT^{cre} mice.

(H) Breeding strategy for generating the Piezo1$^{fl/fl}$Pirt^{GCaMP} and Piezo1$^{fl/fl}$Pirt^{GCaMP}ChAT^{cre} mice.

(I) Schematic overview of the *ex vivo* Ca^{2+} imaging experimental setup.

(J) Representative single frames taken from GCaMP3 fluorescence recordings of neurons within colonic myenteric ganglia from Piezo1$^{fl/fl}$Pirt^{GCaMP} mice before and after mechanical brushing. Responsive neurons are marked with white arrows. Scale bar: 20 μm.

(K) Representative single frames taken from GCaMP3 fluorescence recordings of neurons within the colonic myenteric ganglia from Piezo1$^{fl/fl}$Pirt^{GCaMP}ChAT^{cre} mice before and after mechanical brushing. Scale bar: 20 μm.

(legend continued on next page)

a significant increase in nuclear c-FOS abundance compared with DMSO-treated controls in colon explants (Figures S2G and S2H). Notably, hydrostatic-pressure-induced nuclear c-FOS abundance was dependent on extracellular calcium (Figures S2I and S2J). We crossed Piezo1$^{fl/fl}$ to a pan-ENS expressing-cre,[8,32–34] Hand2^{cre}, and sought to uncover whether enteric neurons in colon explants use Piezo1 to sense pressure alterations. We observed a significant increase in nuclear c-FOS abundance in neurons from colon explants from Piezo1$^{fl/fl}$ mice subjected to cyclical hydrostatic pressure, which was completely abrogated in Piezo1$^{fl/fl}$Hand2^{cre} mice (Figures 2A–2C).

We next conducted whole-cell patch-clamp recordings in Ai9-tdTomato^{+} myenteric neurons isolated from both Ai9$^{fl/fl}$ChAT^{cre} and Piezo1$^{fl/fl}$Ai9$^{fl/fl}$ChAT^{cre} mice to characterize PIEZO1-mediated mechanically activated current (Figures 2D, 2E, S2K, and S2L). Direct mechanical stimulation evoked whole-cell currents in approximately 25.4% of tdTomato^{+} enteric neurons isolated from Ai9$^{fl/fl}$ChAT^{cre} mice, but only in 4.8% of tdTomato^{+} enteric neurons isolated from Piezo1$^{fl/fl}$Ai9$^{fl/fl}$ChAT^{cre} mice (Figures 2F and 2G). Additionally, we generated Piezo1$^{fl/fl}$Pirt^{GCaMP} and Piezo1$^{fl/fl}$Pirt^{GCaMP}ChAT^{cre} mice and detected Yoda1-induced green flourescent protein-based calcium indicator (GCaMP) signals in 19.3% of cultured enteric neurons isolated from Piezo1$^{fl/fl}$Pirt^{GCaMP}, but only in 1.2% of enteric neurons isolated from Piezo1$^{fl/fl}$Pirt^{GCaMP}ChAT^{cre} mice (Figures S2M–S2P). We also measured mechanical brushing-induced GCaMP signals in *ex vivo* whole-mount colon preparations (Figures 2H and 2I). We found that the ablation of Piezo1 from cholinergic neurons resulted in diminished mechanical brushing-induced GCaMP signals in enteric neurons (Figures 2J–2N; Videos S1 and S2). Importantly, shear stress- and Yoda1-induced GCaMP signals were also reduced in whole-mount colon preparations of Piezo1$^{fl/fl}$Pirt^{GCaMP}ChAT^{cre} mice compared with that of Piezo1$^{fl/fl}$Pirt^{GCaMP} mice (Figures S2Q–S2U). In contrast, non-mechanically evoked GCaMP signals to the neurotransmitter 5-HT and KCl neuronal depolarization were intact in Piezo1-deficient cholinergic enteric neurons (Figures S2V–S2Y).

Optogenetic and chemogenetic manipulation of Piezo1^{+} cholinergic enteric neurons regulates intestinal motility

To understand the function of Piezo1^{+} enteric neurons in the colon, we took an intersectional genetic approach and integrated a double gated (loxP and flippase recognition target [FRT]) red-shifted channelrhodopsin-mCitrine (ReaChR) selectively into Piezo1^{+} cholinergic neurons by generating Piezo1^{flpo}ChAT^{cre} ReaChR-mCitrine$^{stop/stop}$ mice (Figure S3A). We observed specific expression of mCitrine fluorescence in ChAT^{+} enteric neurons only when both Piezo1^{flpo} and ChAT^{cre} were co-expressed with ReaChR-mCitrine$^{stop/stop}$ transgene (Figures 3A and S3B). While mCitrine was robustly expressed in ChAT^{+} enteric neurons, no expression was detected in neuron populations in dorsal root, nodose, or celiac ganglia (Figures S3C–S3E). We conducted patch-clamp recordings on both mCitrine^{+} and mCitrine^{-} enteric neurons isolated from Piezo1^{flpo}ChAT^{cre} ReaChR-mCitrine$^{stop/stop}$ mice. Optical stimulation activated robust light-intensity-dependent inward whole-cell currents only in the mCitrine^{+} cells (Figures 3B–3D).

Ex vivo optogenetic stimulation of Piezo1^{+} cholinergic enteric neurons significantly increased CMMC responses in whole colon segments from Piezo1^{flpo}ChAT^{cre}ReaChR-mCitrine$^{stop/stop}$ mice but not controls (Figures 3E–3G, S3F, and S3G). To uncover whether optogenetic activation of Piezo1^{+}ChAT^{+} enteric neurons in freely moving mice could accelerate colonic motility, we employed an implantable wireless device as previously reported.[35] Optogenetic activation of Piezo1^{+} cholinergic enteric neurons reduced the time needed for a glass bead to be expelled from the colons of the Piezo1^{flpo}ChAT^{cre}ReaChR-mCitrine$^{stop/stop}$ mice (Figures 3H–3J).

To understand whether acute inhibition of Piezo1^{+} cholinergic neurons could slow GI motility *in vivo*, we crossed Piezo1^{flpo} ChAT^{cre} mice to a double STOP gated inhibitory designer receptors exclusively activated by designer drugs (DREADD) hM4Di mouse line (Gi).[36] To measure total GI transit in Piezo1^{flpo}ChAT^{cre}Gi and control mice treated with clozapine N-oxide (CNO), we gavaged mice with carmine red food dye and measured the time delay for the first red fecal pellet to be expelled. Inhibition of Piezo1^{+}ChAT^{+} neurons resulted in significantly reduced intestinal motility (Figure 3K). Furthermore, we also assessed GI transit by measuring the distribution of an orally administered fluorescein isothiocyanate (FITC)-dextran along the GI tract of Piezo1^{flpo}ChAT^{cre}Gi and control mice treated with CNO. Inhibition of Piezo1^{+}ChAT^{+} neuronal activity resulted in decreased intestinal motility (Figure 3L). Finally, we tested whether Piezo1 activity in cholinergic neurons was also required to accelerate colonic transit by inserting a glass bead into the colon of Piezo1^{flpo}ChAT^{cre}Gi and control mice. Acute disruption of Piezo1^{+}ChAT^{+} neuronal activity significantly delayed colonic glass bead expulsion (Figure 3M).

Cholinergic enteric neurons detect luminal pressures to regulate colon motility through Piezo1

Muscle tension recording showed that colon strips from Piezo1$^{fl/fl}$ChAT^{cre} mice exhibited compromised peristaltic contraction compared with those from Piezo1$^{fl/fl}$ mice (Figure 4A; quantified in Figures 4B–4D). Although the CMMC frequencies were not significantly different between colon preparations from Piezo1$^{fl/fl}$ and Piezo1$^{fl/fl}$ChAT^{cre} mice at 2 cmH_2O luminal pressure, colon preparations from the Piezo1$^{fl/fl}$ChAT^{cre} mice showed a significantly reduced CMMC frequency compared

(L) Quantification of enteric neurons activated by mechanical brushing stimulation per field of view from Piezo1$^{fl/fl}$Pirt^{GCaMP} and Piezo1$^{fl/fl}$Pirt^{GCaMP}ChAT^{cre} mice.
(M) Representative time-lapse Ca^{2+} imaging traces of mechanical brushing-induced [Ca^{2+}]i response in the whole-mount myenteric plexus enteric neurons from Piezo1$^{fl/fl}$Pirt^{GCaMP} mice.
(N) Representative time-lapse Ca^{2+} imaging traces of mechanical brushing-induced [Ca^{2+}]i response in whole-mount myenteric plexus enteric neurons from Piezo1$^{fl/fl}$Pirt^{GCaMP}ChAT^{cre} mice.
Statistics determined by two-tailed Student's t test. ns, no significant difference, $^{*}p < 0.05$, $^{**}p < 0.01$, $^{***}p < 0.001$, $^{****}p < 0.0001$.
See also Figure S2.

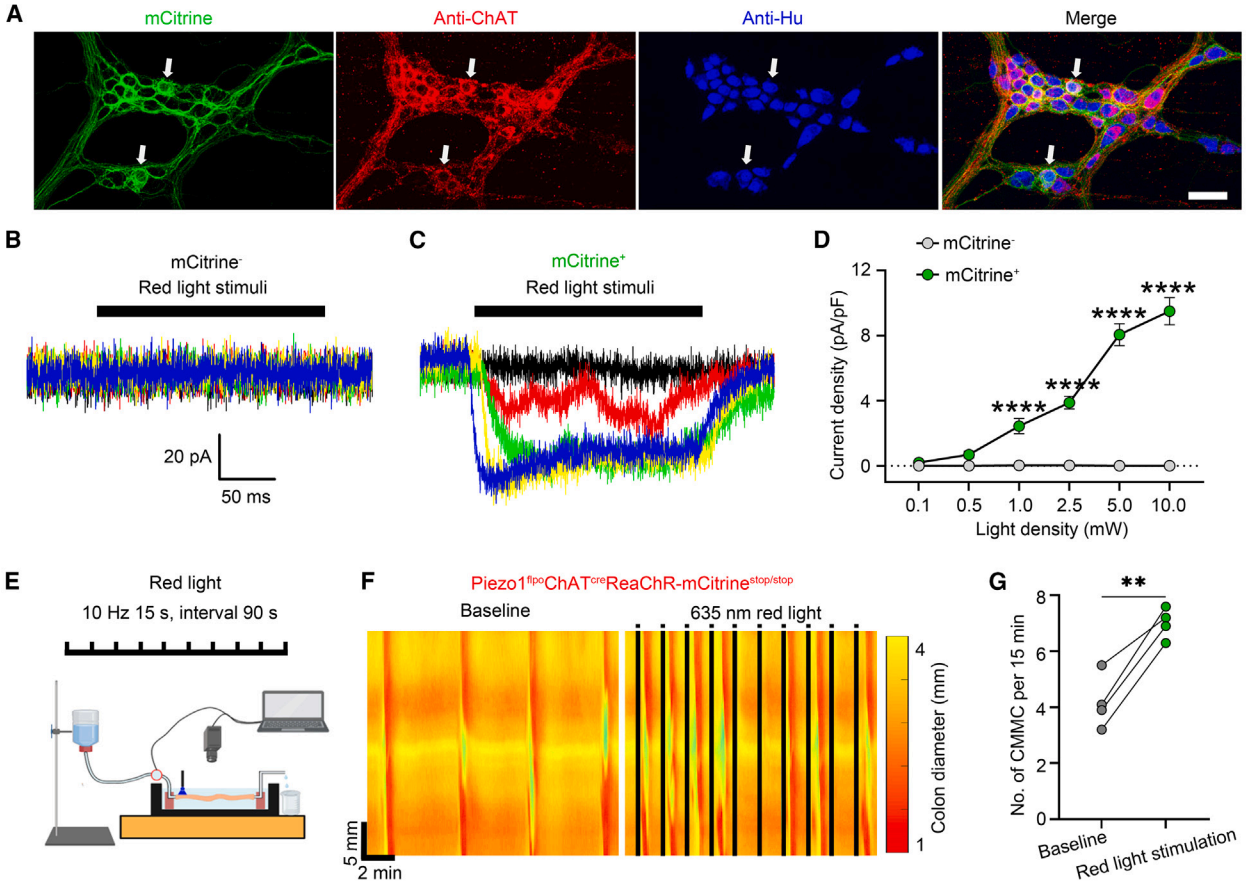

(legend on next page)

with that from Piezo1$^{fl/fl}$ mice at 4 cmH_2O luminal pressure (Figures 4E and 4F). Interestingly, increased luminal pressure from 2 to 4 cmH_2O could enhance CMMC frequency in colon preparations from both Piezo1$^{fl/fl}$ mice and Piezo1$^{fl/fl}$ChAT^{cre} mice; however, the rising luminal pressure-enhanced CMMC was significantly higher in the colon of Piezo1$^{fl/fl}$ mice when compared with that in Piezo1$^{fl/fl}$ChAT^{cre} mice (Figures 4F and 4G). Additionally, the velocity of the glass bead movement was significantly slower in the colon preparations from Piezo1$^{fl/fl}$ ChAT^{cre} mice compared with control animals (Figures 4H–4J).

Piezo1 is required for excitatory cholinergic enteric neurons to accelerate GI transit

Before using Hand2^{cre} and ChAT^{cre} for loss-of-function GI motility studies *in vivo*, we conducted a careful assessment of the expression of *Piezo1*, *Chat*, and *Hand2* in both intrinsic and extrinsic neuron populations. We identified that *Piezo1* is highly expressed in enteric neurons compared with all other neuron populations, and only co-expresses with *Hand2* or *Chat* in enteric neuronal populations[37] (Figure S4A). As previously reported,[12] *Piezo2* was highly expressed in extrinsic sensory neurons that innervate the colon, while *Piezo1*, *Chat*, and *Hand2* all showed limited expression[38] (Figures S4A and S4B). Mining enteric glial scRNA-seq data[25] revealed that although *Piezo2* was highly expressed, *Piezo1* and *Chat* were undetectable (Figure S4C). Analysis of sympathetic neurons isolated from the celiac ganglia revealed no expression of *Piezo1*, *Piezo2*, or *Chat* expression (Figure S4D). Finally, although tuft cells also express *Chat*,[39,40] we identified that these intestinal epithelial cells do not express Piezo1[41] (Figures S4E and S4F).

Loss of Piezo1 expression in both enteric and cholinergic myenteric neurons resulted in reduced neuronal activity (Figures 5A, 5B, S4G, and S4H). Deletion of Piezo1 in the ENS resulted in a significantly delayed appearance of carmine red compared with littermate controls (Figure 5C). In agreement, loss of Piezo1 in cholinergic neurons also resulted in slower total GI transit than control mice (Figure 5D). Notably, the length of the GI tract was not different between Piezo1$^{fl/fl}$ and Piezo1$^{fl/fl}$ ChAT^{cre} mice (Figure S4I). GI transit was also significantly reduced in Piezo1$^{fl/fl}$ChAT^{cre} mice when compared with Piezo1$^{fl/fl}$ mice using the FITC-dextran assay (Figures 5E and 5F). We also found Piezo1$^{fl/fl}$ChAT^{cre} mice needed a significantly longer time to expel a glass bead when compared with controls (Figure 5G). Moreover, the Piezo1$^{fl/fl}$ChAT^{cre} mice had significantly reduced water content of freshly expelled fecal pellets when compared with controls (Figure 5H).

In contrast, conditional knockout of Piezo1 from inhibitory enteric neurons by crossing Piezo1$^{fl/fl}$ mice with Nos1$^{ERT2\text{-}cre}$ or Vip^{cre} mice did not affect GI transit, colon transit, or colon length compared with controls (Figures S4J–S4M). Additionally, whole GI transit, colon motility, and colon length were comparable between Piezo2$^{fl/fl}$Hand2^{cre} mice and Piezo2$^{fl/fl}$ChAT^{cre} and their own littermate controls (Figures S4N–S4Q).

Loss of Piezo1 in the ENS, had no effect on body mass, food or water consumption compared with their controls (Figures S5A–S5H). Likewise, loss of Piezo1 in ChAT positive cells also resulted in no observable defect in the number of neurons, or the distribution of excitatory and inhibitory neurons in the GI tract (Figures S5I–S5M). To avoid potential developmental defects, we next investigated whether loss of Piezo1 in cholinergic colonic enteric neurons in adult mice disrupted motility. We injected an AAV$^{GFP\text{-}cre}$ virus or control virus (AAV^{GFP}) driven by the ChAT promoter into the colon wall of Piezo1$^{fl/fl}$ mice (Figure 5I). After validating the expression of GFP in enteric cholinergic neurons (Figure 5J), we performed both *ex vivo* and *in vivo* colon motility assays and the Piezo1$^{AAV\text{-}GFP\text{-}cre}$ mice showed significantly reduced colon motility compared with Piezo1$^{AAV\text{-}GFP}$ control mice (Figures 5K–5M). Moreover, the total *in vivo* GI transit time was increased in Piezo1$^{AAV\text{-}GFP\text{-}cre}$ mice compared with Piezo1$^{AAV\text{-}GFP}$ mice (Figure 5N).

Finally, to test for any role for sympathetic neurons in Piezo1-dependent GI transit, we ablated sympathetic neurons using

Figure 3. Optogenetic and chemogenetic manipulation of Piezo1^{+} cholinergic enteric neurons regulates intestinal motility

(A) Immunofluorescent images showing mCitrine expression in enteric neurons from a whole-mount preparation of the longitudinal muscle layer in the colon of a Piezo1^{flpo}ChAT^{cre}ReaChR-mCitrine$^{stop/stop}$ mouse, co-stained for anti-ChAT and anti-Hu. Scale bar: 25 μm.

(B) Representative whole-cell membrane current traces evoked by red light illumination in a mCitrine^{-} myenteric neuron isolated from a Piezo1^{flpo}ChAT^{cre} ReaChR-mCitrine$^{stop/stop}$ mouse.

(C) Representative whole-cell membrane current traces evoked by red light illumination in a mCitrine^{+} myenteric neuron isolated from a Piezo1^{flpo}ChAT^{cre} ReaChR-mCitrine$^{stop/stop}$ mouse.

(D) Quantification of red light-activated currents in mCitrine^{-} and mCitrine^{+} myenteric neurons isolated from Piezo1^{flpo}ChAT^{cre}ReaChR-mCitrine$^{stop/stop}$ mice. Data are expressed as mean ± SE, ****$p < 0.0001$, two-way ANOVA with Bonferroni post hoc analysis.

(E) Schematic of CMMC recording and red-light optogenetic setup.

(F) Representative spatiotemporal maps of CMMC recordings in a colon prep isolated from a Piezo1^{flpo}ChAT^{cre}ReaChR-mCitrine$^{stop/stop}$ mouse, with and without red light.

(G) Quantification of CMMC frequencies within a 15-min duration under both baseline and red-light stimulation in Piezo1^{flpo}ChAT^{cre}ReaChR-mCitrine$^{stop/stop}$ mice.

(H) Schematic of *in vivo* optogenetic stimulation of colon transit.

(I) Quantification of colon transit time under both baseline and red-light stimulation conditions in WT mice.

(J) Quantification of colon transit time under both baseline and red light stimulation conditions in Piezo1^{flpo}ChAT^{cre}ReaChR-mCitrine$^{stop/stop}$ mice.

(K) Summary data showing *in vivo* GI transit via carmine red assay in control and Piezo1^{flpo}ChAT^{cre}Gi mice.

(L) Summary data showing *in vivo* GI transit using FITC-dextran in control and Piezo1^{flpo}ChAT^{cre}Gi mice.

(M) Quantification of *in vivo* colon transit time using a glass bead in control and Piezo1^{flpo}ChAT^{cre}Gi mice.

Unless otherwise stated, statistics were determined by two-tailed Student's t test. ns, no significant difference, *$p < 0.05$, **$p < 0.01$, ***$p < 0.001$, ****$p < 0.0001$. See also Figure S3.

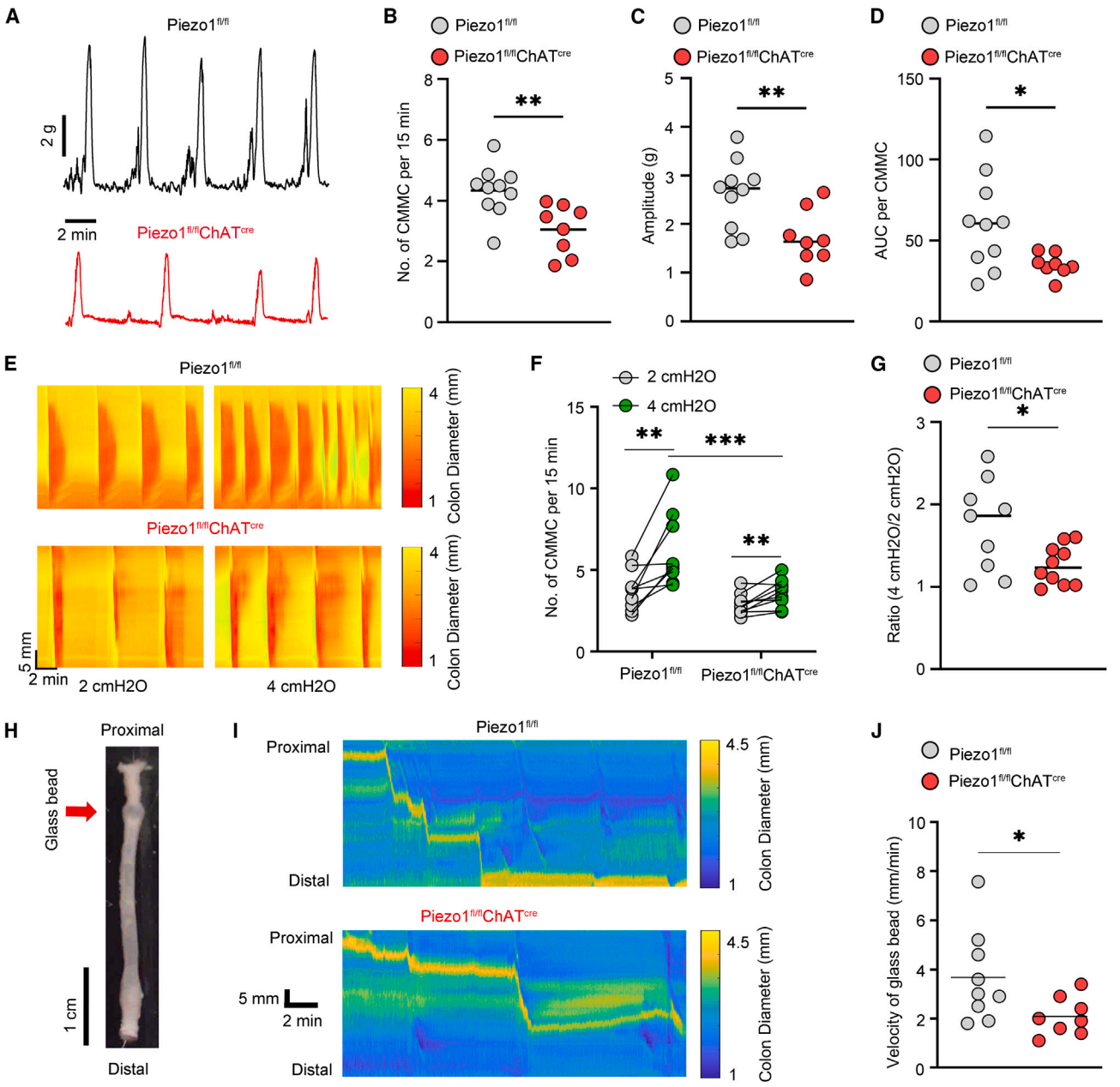

Figure 4. Cholinergic enteric neurons detect luminal pressures to regulate colon motility through Piezo1

(A) Representative traces of tension recording from a colon prep of Piezo1$^{fl/fl}$ mouse and a colon prep of Piezo$^{fl/fl}$ChAT^{cre} mouse.

(B) Quantification of CMMC frequencies within a 15 min in colon preps from Piezo1$^{fl/fl}$ and Piezo1$^{fl/fl}$ChAT^{cre} mice.

(C) Mean CMMC contraction parameters of amplitude in colon preps from Piezo1$^{fl/fl}$ and Piezo1$^{fl/fl}$ChAT^{cre} mice.

(D) Mean CMMC contraction parameters of area under the curve (AUC) in colon preps from Piezo1$^{fl/fl}$ and Piezo1$^{fl/fl}$ChAT^{cre} mice.

(E) Representative spatiotemporal maps illustrating CMMCs from a colon prep of Piezo1$^{fl/fl}$ mouse and a colon prep of Piezo$^{fl/fl}$ChAT^{cre} mouse under 2 and 4 cmH_2O pressures.

(F) Quantification of CMMCs within a 15-min duration in colon preps from Piezo1$^{fl/fl}$ and Piezo1$^{fl/fl}$ChAT^{cre} mice under 2 and 4 cmH_2O pressures.

(G) Ratios of the numbers of CMMCs within a 15-min duration under 4 and 2 cmH_2O pressures in colon preps from Piezo1$^{fl/fl}$ and Piezo1$^{fl/fl}$ChAT^{cre} mice.

(H) Schematic of *ex vivo* colon transit experiment setup.

(I) Representative spatiotemporal maps illustrating colon transit in a colon prep from a Piezo1$^{fl/fl}$ mouse and a Piezo1$^{fl/fl}$ChAT^{cre} mouse.

(J) Velocity of glass bead movement in colon preps from Piezo1$^{fl/fl}$ mice and Piezo1$^{fl/fl}$ChAT^{cre} mice.

Statistics determined by two-tailed Student's t test. ns, no significant difference, $*p < 0.05$, $**p < 0.01$, $***p < 0.001$, $****p < 0.0001$.

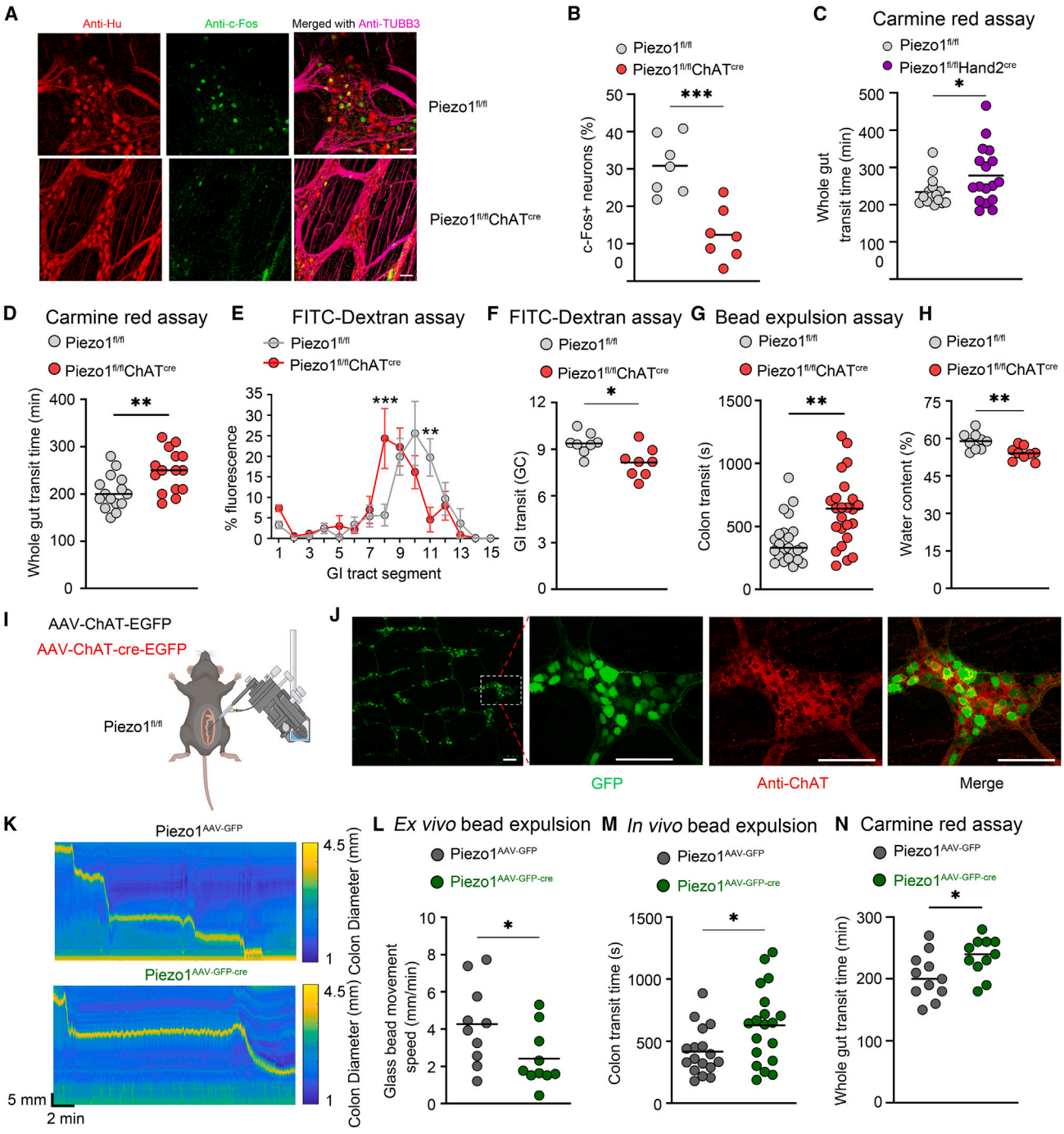

Figure 5. Piezo1 is required for excitatory cholinergic enteric neurons to accelerate GI transit

(A) Immunofluorescence image of isolated colonic myenteric plexus stained for anti-Hu, anti-c-Fos, and anti-beta tubulin 3 from Piezo1$^{fl/fl}$ and Piezo1$^{fl/fl}$ChAT^{cre} mice. Scale bar: 78 μm.

(B) Quantification of the ratio of c-Fos^{+} neuron cell bodies to total neuron cell bodies stained in (A).

(C) Summary data showing *in vivo* GI transit via carmine red assay in Piezo1$^{fl/fl}$ and Piezo1$^{fl/fl}$Hand2^{cre} mice.

(D) Summary data showing *in vivo* GI transit via carmine red assay in Piezo1$^{fl/fl}$ and Piezo1$^{fl/fl}$ChAT^{cre} mice.

(E) Distribution of FITC-dextran in luminal contents of stomach and 10 small intestinal segments, cecum, and 3 colonic segments after FITC-dextran dye gavage of Piezo1$^{fl/fl}$ and Piezo1$^{fl/fl}$ChAT^{cre} mice. Data are expressed as mean ± SE. $^{**}p < 0.01$, $^{***}p < 0.001$, two-way ANOVA with Bonferroni post hoc analysis. $n = 8$ mice per group.

(F) Summary data showing *in vivo* GI transit via FITC-dextran assay in Piezo1$^{fl/fl}$ and Piezo1$^{fl/fl}$ChAT^{cre} mice

(G) Quantification of *in vivo* colon transit time via glass bead assay in Piezo1$^{fl/fl}$ and Piezo1$^{fl/fl}$ChAT^{cre} mice.

(legend continued on next page)

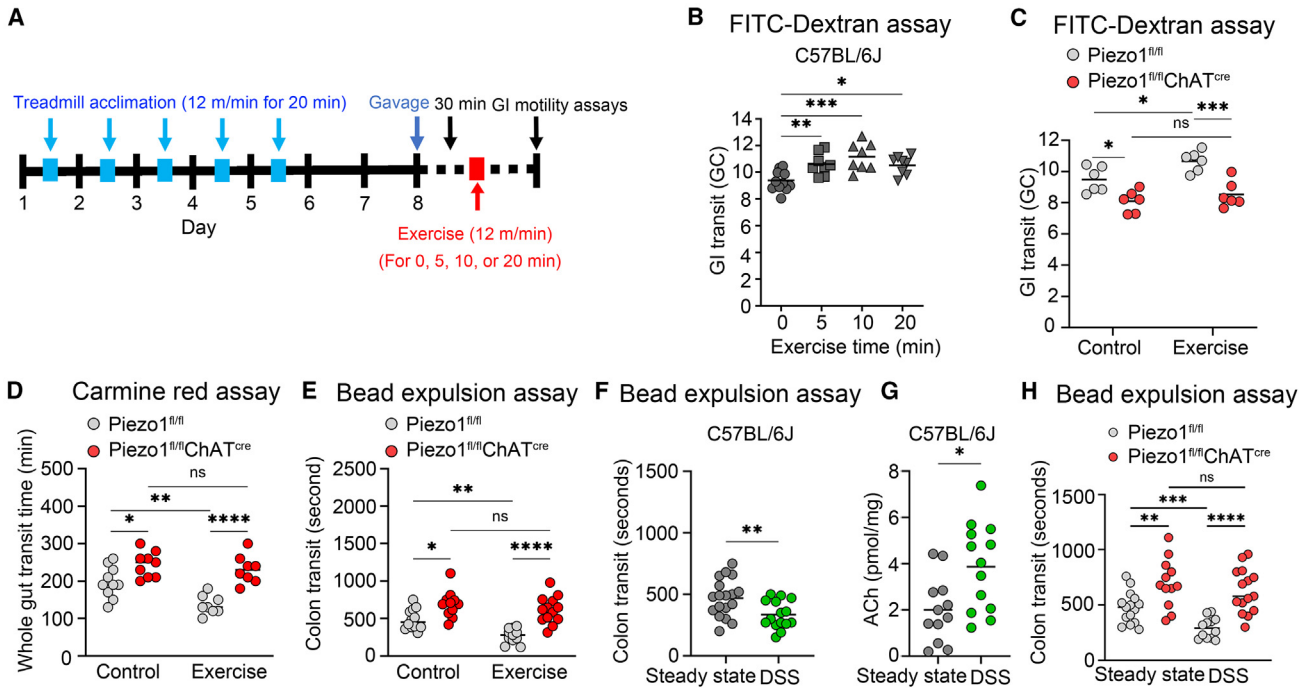

Figure 6. Piezo1 in enteric cholinergic neurons is required for exercise- and inflammation-accelerated GI motility

(A) Schematic of treadmill exercise protocol.

(B) Summary data illustrating the impact of different treadmill exercise duration on GI transit via FITC-dextran assay in C57BL/6J mice. *$p < 0.05$, **$p < 0.01$, ***$p < 0.001$, one-way ANOVA.

(C) Summary data showing the impact of 10-min treadmill exercise on GI transit via FITC-dextran assay in Piezo1$^{fl/fl}$ and Piezo1$^{fl/fl}$ChAT^{cre} mice.

(D) Summary data showing the impact of 10-min treadmill exercise on whole gut GI transit via carmine red assay in Piezo1$^{fl/fl}$ and Piezo1$^{fl/fl}$ChAT^{cre} mice. ns, no significant difference, *$p < 0.05$, **$p < 0.01$, ****$p < 0.0001$ one-way ANOVA.

(E) Summary data showing the impact of 10-min treadmill exercise on colon transit via bead expulsion assay in Piezo1$^{fl/fl}$ and Piezo1$^{fl/fl}$ChAT^{cre} mice. ns, no significant difference, *$p < 0.05$, **$p < 0.01$, ****$p < 0.0001$ one-way ANOVA.

(F) Quantification of *in vivo* colon transit time via bead expulsion assay in WT mice at steady state compared with day 2 of 2.5% DSS.

(G) Quantification of ACh measured from colons of WT mice at steady state compared with day 2 of 2.5% DSS.

(H) Quantification of *in vivo* colon transit time via bead expulsion assay in Piezo1$^{fl/fl}$ and Piezo1$^{fl/fl}$ChAT^{cre} mice at steady state compared with day 2 of 2.5% DSS.

Unless otherwise stated, statistics were determined by two-tailed Student's t test. ns, no significant difference, *$p < 0.05$, **$p < 0.01$, ***$p < 0.001$, ****$p < 0.0001$. See also Figure S6.

6-hydroxydopamine (6-OHDA) treatment (Figures S5N and S5O). As expected, 6-OHDA treatment resulted in accelerated GI transit in Piezo1$^{fl/fl}$ animals as sympathetic neurons are known to slow intestinal motility[42] (Figure S5P). Importantly, however, even in the absence of sympathetic innervation, loss of Piezo1 in cholinergic neurons still resulted in decreased GI motility compared with 6-OHDA treated Piezo1$^{fl/fl}$ control mice (Figure S5P).

Piezo1 in enteric cholinergic neurons is required for exercise- and inflammation-accelerated GI motility

Given that exercise could potentially enhance intra-abdominal pressure and/or organ bouncing, we hypothesized that exercise activates Piezo1^{+} cholinergic enteric neurons to promote gut motility. To test this hypothesis, we conducted a treadmill exercise protocol in mice (Figure 6A). As predicted, a significant increase in GI transit during treadmill exercise was observed,

(H) Water content of fecal pellets from Piezo1$^{fl/fl}$ and Piezo1$^{fl/fl}$ChAT^{cre} mice.

(I) Schematic of Piezo1$^{fl/fl}$ mice subjected to intracolonic injections with ChAT-promoter-driven AAV^{GFP} control or AAV$^{GFP\text{-}cre}$ virus.

(J) Representative images illustrate the presence of GFP^{+} myenteric neurons in mice that have been injected with ChAT-promoter-driven AAV encoding GFP. The three enlarged images on the right, which are derived from the boxed area in the low magnification image on the left. Scale bar: 100 μm.

(K) Representative spatiotemporal maps illustrating glass bead movement in colon preps from Piezo1$^{AAV\text{-}GFP}$ and Piezo1$^{AAV\text{-}GFP\text{-}cre}$ mice.

(L) Quantification of *ex vivo* glass bead movement in colon preps from Piezo1$^{AAV\text{-}GFP}$ and Piezo1$^{AAV\text{-}GFP\text{-}cre}$ mice.

(M) Quantification of *in vivo* colon transit time via glass bead expulsion assay in Piezo1$^{AAV\text{-}GFP}$ and Piezo1$^{AAV\text{-}GFP\text{-}cre}$ mice measured by inserting a 3 mm glass bead into the colon.

(N) Summary data showing *in vivo* GI transit via carmine red assay in Piezo1$^{AAV\text{-}GFP}$ and Piezo1$^{AAV\text{-}GFP\text{-}cre}$ mice.

Unless otherwise stated, statistics were determined by two-tailed Student's t test. ns, no significant difference, *$p < 0.05$, **$p < 0.01$, ***$p < 0.001$, ****$p < 0.0001$. See also Figures S4 and S5.

which peaked at the 10-min exercise duration (Figure 6B). Importantly, the 10 min exercise-enhanced GI motility was abolished in Piezo1$^{fl/fl}$ChAT^{cre} mice (Figures 6C–6E). Note that Piezo1 deficiency from cholinergic neurons had no significant effect on voluntary movement (Figures S6A–S6D). To investigate whether sympathetic neurons were operative during treadmill exercise, we administered Piezo1$^{fl/fl}$ChAT^{cre} mice and littermate controls with 6-OHDA. While sympathetic denervation resulted in accelerated GI transit in control mice, the defect in Piezo1-deficient cholinergic neurons was still apparent in these animals, indicative that Piezo1-activity is independent of sympathetic innervation (Figure S6E).

In addition to exercise, inflammation is known to alter GI motility and can result in diarrhea in patients with IBD.[43] Consistent with this, we subjected wild-type (WT) mice to a chemically induced colitis model using dextran sodium sulfate (DSS) in drinking water for 2 days and observed accelerated colonic transit concurrent with elevated acetylcholine levels in intestinal tissue (Figures 6F and 6G). To test whether mechanosensation by Piezo1 in cholinergic neurons was required for the DSS-associated increase in colonic motility, we administered DSS to both Piezo1$^{fl/fl}$ and Piezo1$^{fl/fl}$ChAT^{cre} mice. Remarkably, while WT mice increased transit rate during DSS-induced colitis, loss of Piezo1 in ChAT^{+} neurons showed retarded colonic transit that failed to accelerate during colitis (Figure 6H).

Cholinergic enteric neuronal Piezo1-mechanosensation protects against colitis

Loss of Piezo1 in cholinergic and enteric neurons results in decreased levels of acetylcholine (ACh) in colonic tissue (Figures 7A and 7B). As ACh is not only excitatory at neuromuscular junctions but also anti-inflammatory at the mucosa,[44] we next assessed colitis severity and inflammation. Loss of Piezo1 in enteric and cholinergic neurons results in a dramatic susceptibility to colitis-induced weight loss (Figures 7C and 7D) and colonic shortening (Figures 7E and 7F) compared with controls. This was accompanied by a colitis-induced progressive loss of luminal mucus and protective goblet cell numbers in the Piezo1-deficient animals compared with control mice (Figures 7G–7J and S7A–S7D). We also observed prolonged, unresolved inflammation up to 1 month post DSS administration as measured by the IBD fecal biomarker lipocalin-2 (LCN2) in Piezo1-deficient mice (Figures S7E and S7F). As myeloid cells are the major producers of LCN2, we imaged colon sections of Piezo1$^{fl/fl}$ChAT^{cre} and Piezo1$^{fl/fl}$Hand2^{cre} on day 8 of DSS. We observed increased CD11b^{+} myeloid cells in mice lacking neuronal-Piezo1 expression compared with littermate controls (Figures S7G–S7J). Flow cytometric analysis from colonic immune cells confirmed a significant increase in infiltrating inflammatory monocytes in both Piezo1$^{fl/fl}$ChAT^{cre} and Piezo1$^{fl/fl}$Hand2^{cre} mice compared with their Piezo1$^{fl/fl}$ control mice (Figures 7K–7M, and S7K–S7X). Conversely, loss of Piezo1 in enteric glial cells had no effect on colitis-induced severity (Figures S7Y–S7AA). Similarly, loss of Piezo1 in inhibitory neurons expressing VIP had no effect on DSS-induced colitis (Figures S7AB and S7AC). Moreover, by using Piezo2$^{fl/fl}$ and Piezo2$^{fl/fl}$Hand2^{cre} littermates, we found that loss of Piezo2 in the ENS had no effect on colitis severity (Figures S7AD and S7AE).

To avoid the possibility that developmental defects were responsible for the increased severity observed in Piezo1-knockout mice, we utilized AAV-delivery of ChAT^{cre} to ablate expression of Piezo1 in cholinergic colonic neurons in Piezo1$^{fl/fl}$ mice. Loss of Piezo1 in adult animals also increased susceptibility to DSS-induced weight loss (Figure 7N), colonic shortening (Figure 7O), colonic inflammation (Figure S7AF), and decreased colonic ACh levels (Figure 7P). To test whether acute inhibition of Piezo1^{+} cholinergic enteric neurons could also exacerbate DSS-induced colitis, we subjected Piezo1^{flpo}ChAT^{cre}Gi and control mice to DSS-induced colitis. Administration of CNO in Piezo1^{flpo}ChAT^{cre}Gi mice triggered increased weight loss (Figure 7Q), colonic shortening (Figure 7R), and increased levels of fecal LCN2 (Figure S7AG). Remarkably, the inhibition of Piezo1^{+}ChAT^{+} neurons resulted in decreased colonic ACh levels (Figure 7S), suggesting that Piezo1^{+} cholinergic neurons control ACh release *in vivo*. Finally, to test whether mechanosensation by Piezo1 in enteric neurons can directly trigger ACh release, we subjected enteric neuron cultures to hydrostatic pressure and observed an increase in ACh release compared with neurons cultured in ambient pressure conditions. Importantly, pharmacological blockade of Piezo1 using the antagonist GsMTx4 prevented hydrostatic-pressure-induced release of ACh from neurons (Figure 7T).

DISCUSSION

Mechanosensitivity in the GI tract is essential to normal GI physiology and dysregulated mechanosensing by extrinsic neurons causes GI dysmotility and visceral pain.[15,45,46] Recently, Piezo2 in Nav1.8^{+} dorsal root ganglia (DRGs) neurons was found to be necessary for sensing gut content and can slow down food transit rates throughout the GI tract.[12] Our study uncovered a pivotal role of enteric neuronal Piezo1 for sensing luminal pressure to accelerate gut motility. Together, these observations unravel a complex mechanosensory system that has evolved to control digestion in which Piezo1 expression on cholinergic enteric neurons can sense pressure to accelerate motility, while Piezo2 on extrinsic innervating neurons can retard motility. It can be speculated that for a system as essential to life as digestion, it may be advantageous for its control to be governed by both intrinsic and extrinsic nervous systems and two evolutionarily related Piezo proteins. Interestingly, in addition to the GI tract, several other mechanically diverse organ systems such as the heart[47] and the lung[48] have not only extrinsic innervation, but intrinsic neuronal circuits akin to the ENS in the intestine. The possibility that intrinsic neuronal Piezo1 broadly acts as an internal sentinel of mechanical force within a tissue, while extrinsic somatosensory mechanosensation via Piezo2 universally acts as an external surveyor of force by the CNS in different organ systems, is an exciting prospect.

In addition to the nervous system, Piezo proteins have been reported to play important roles in the GI tract. For example, selective deletion of Piezo1 from the intestinal epithelium has been reported to significantly disrupt intestinal peristalsis.[23] Interestingly, Fang et al. also showed that mice with goblet-cell-specific Piezo1 deficiency exhibit reduced mucus synthesis and disrupted intestinal transit.[49] Thus, the precise roles of the Piezo family of proteins

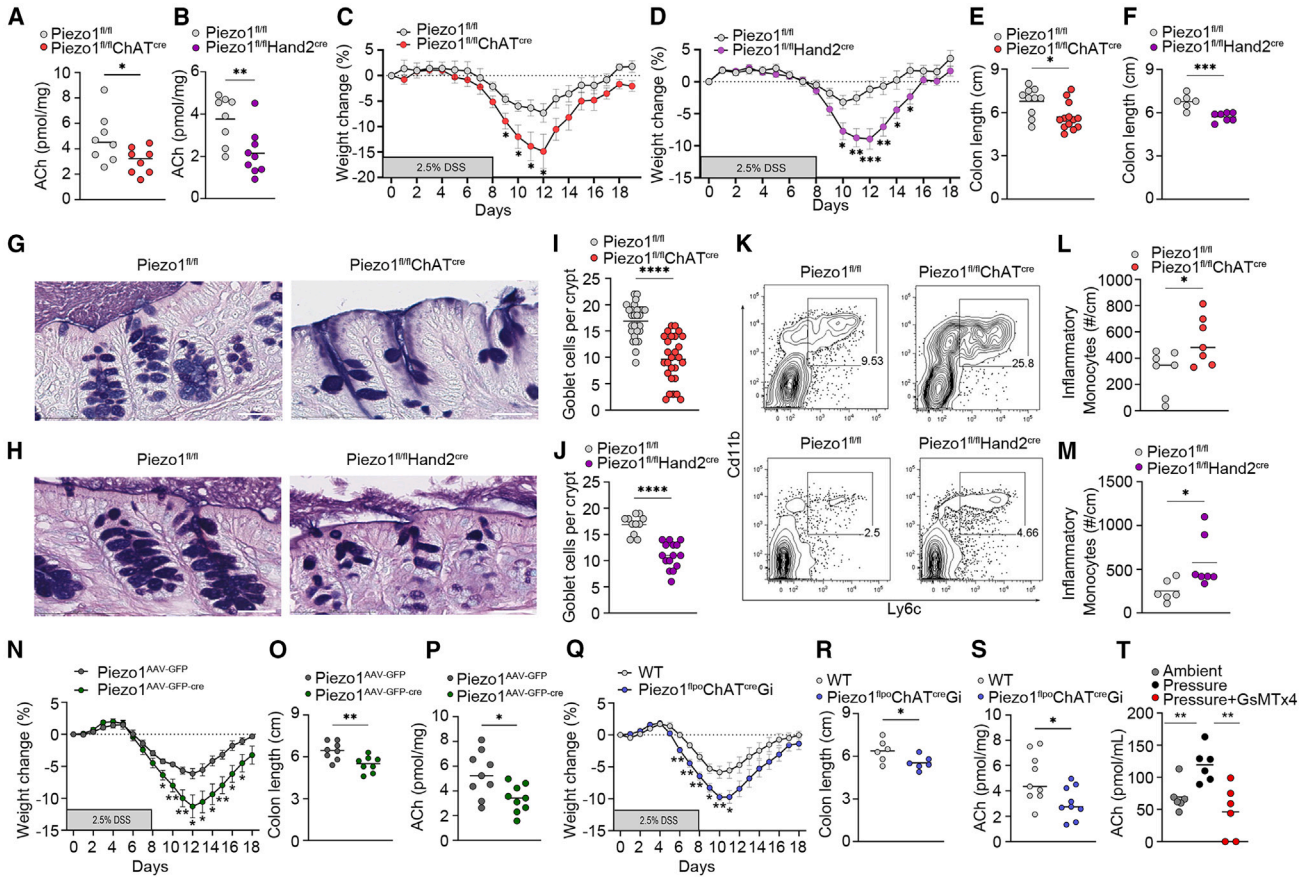

Figure 7. Cholinergic enteric neuronal Piezo1-mechanosensation protects against colitis

(A) Quantification of ACh measured from colons of Piezo1$^{fl/fl}$ and Piezo1$^{fl/fl}$ChAT^{cre} mice at steady state.

(B) Quantification of ACh measured from colons of Piezo1$^{fl/fl}$ and Piezo1$^{fl/fl}$Hand2^{cre} mice at steady state.

(C) Weight loss of cohoused Piezo1$^{fl/fl}$ (n = 10) and Piezo1$^{fl/fl}$ChAT^{cre} (n = 10) mice. Mice were administered 2.5% DSS in their drinking water for 8 days. Data are expressed as mean ± SE.

(D) Weight loss of cohoused Piezo1$^{fl/fl}$ (n = 23) and Piezo1$^{fl/fl}$Hand2^{cre} (n = 28) mice. Mice were administered 2.5% DSS in their drinking water for 8 days. Data are expressed as mean ± SE.

(E) Summary data of colon length shortening post DSS administration in Piezo1$^{fl/fl}$ and Piezo1$^{fl/fl}$ChAT^{cre} cohoused mice on day 8 post DSS treatment.

(F) Summary data of colon length shortening post DSS administration in Piezo1$^{fl/fl}$ and Piezo1$^{fl/fl}$Hand2^{cre} cohoused mice on day 8 post DSS treatment.

(G) Representative AB/PAS staining of colon sections obtained from cohoused Piezo1$^{fl/fl}$ and Piezo1$^{fl/fl}$ChAT^{cre} littermates on day 8 post DSS treatment. Scale bar: 100 μm.

(H) Representative AB/PAS staining of colon sections obtained from cohoused Piezo1$^{fl/fl}$ and Piezo1$^{fl/fl}$Hand2^{cre} littermates and on day 8 post DSS treatment. Scale bar: 100 μm.

(I) Enumeration of goblet cells per crypt in AB/PAS histological sections from cohoused Piezo1$^{fl/fl}$ and Piezo1$^{fl/fl}$ChAT^{cre} mice

(J) Enumeration of goblet cells per crypt in AB/PAS histological sections from cohoused Piezo1$^{fl/fl}$ and Piezo1$^{fl/fl}$Hand2^{cre} mice.

(K) Flow cytometric assessment of recruited inflammatory monocytes (CD11b^{+}Ly6C^{+}) in Piezo1$^{fl/fl}$ and Piezo1$^{fl/fl}$ChAT^{cre} and Piezo1$^{fl/fl}$ and Piezo1$^{fl/fl}$Hand2^{cre} mice post 8-day administration of DSS.

(L) Summary data of the number of inflammatory monocytes per colon length recruited in Piezo1$^{fl/fl}$ and Piezo1$^{fl/fl}$ChAT^{cre} mice post 8-day administration of DSS.

(M) Summary data of the number of inflammatory monocytes per colon length recruited in Piezo1$^{fl/fl}$ and Piezo1$^{fl/fl}$Hand2^{cre} mice post 8-day administration of DSS.

(N) Weight loss of cohoused Piezo1$^{AAV\text{-}GFP}$ (n = 8) and Piezo1$^{AAV\text{-}GFP\text{-}cre}$ (n = 8) mice. Mice were administered 2.5% DSS in their drinking water for 8 days. Data are expressed as mean ± SE.

(O) Summary data of colon length shortening post DSS administration in cohoused Piezo1$^{AAV\text{-}GFP}$ and Piezo1$^{AAV\text{-}GFP\text{-}cre}$ mice.

(P) Quantification of ACh measured from colons of Piezo1$^{AAV\text{-}GFP}$ and Piezo1$^{AAV\text{-}GFP\text{-}cre}$ mice at steady state.

(Q) Weight loss of cohoused WT (n = 6) and Piezo1^{flpo}ChAT^{cre}Gi (n = 6) mice. Mice were administered 2.5% DSS in their drinking water for 8 days. Data are expressed as mean ± SE.

(R) Summary data of colon length shortening post 8-day administration of DSS in WT and Piezo1^{flpo}ChAT^{cre}Gi cohoused mice.

(S) Quantification of ACh measured from colons of WT and Piezo1^{flpo}ChAT^{cre}Gi mice at steady state.

(T) Quantification of ACh released from differentiated enteric neurons when stimulated with ambient conditions, pressure conditions, or pressure with Piezo1 antagonist GsMTx4.

Statistics were determined by two-tailed Student's t test. ns, no significant difference, *p < 0.05, **p < 0.01, ***p < 0.001, ****p < 0.0001.

See also Figure S7.

across all the different cell types that comprise mechanical organs such as the intestine and how they regulate the global function of these organs in response to force is an exciting area of investigation, which is only beginning to be elucidated.

Recently, appreciation for the role of mechanosensation in the control of inflammation, immunity, and cancer has gained increasing attention.[4,50–52] We previously identified that Piezo1 was essential for myeloid cells to sense pressure to drive inflammatory responses in the lung.[8] Conversely, in this current study, we have found that enteric neurons also use mechanosensation by the same Piezo protein to limit inflammation during colitis. These studies together suggest mechanosensation is intimately intertwined in neuro-immune responses and how force is converted into immunologically relevant outputs may be context and cell-type specific. While new tools will need to be developed, investigating how different mechanosensitive cells respond to force simultaneously in a tissue, and understanding how these cells integrate this information may prove highly informative and provide a deeper understanding of how force impacts inflammatory processes in the body.

Conclusion

Our results have identified how the ENS directly senses luminal pressure at the molecular level. We demonstrate that Piezo1 is selectively and functionally expressed in the ENS and required for maintaining peristalsis, enhancing GI motility during exercise, and preventing tissue destruction in murine models of IBD. By using an intersectional genetic strategy, we showed that the Piezo1^{+} cholinergic excitatory neurons in the ENS serve as the long-sought mechanosensor in detecting pressure in the GI tract and are necessary and sufficient for maintaining normal GI motility and inflammatory homeostasis *in vivo*.

Limitations of the study

While we conclude that mechanical force activates Piezo1^{+} cholinergic neurons which leads to the release of ACh to regulate both intestinal motility and colonic inflammation, we did not directly measure ACh release *in situ* in live tissue. Instead, we demonstrated that pressure could directly trigger ACh release in enteric neuron cultures and that the antagonist GsMTx4 could block this release. While GsMTx4 targets Piezo1 and Piezo1 is the major mechanosensory expressed in enteric neurons, it can also block other mechanosensitive proteins such as Piezo2 and Trek channels; therefore, the contribution of other mechanosensitive channels in this release cannot be fully excluded. Future studies using an ACh biosensor, or the generation of fluorescent or luminescent ACh reporter systems to directly measure real-time ACh release *in vivo* in peripheral neurons, would be exceptionally useful in addressing this limitation. In addition, although we uncovered that exercise induces Piezo1-dependent acceleration of GI motility, due to technical challenges, we were unable to assess whether this is due to increased luminal pressure or from organ bouncing. Furthermore, while enteric neuronal Piezo1 plays a pivotal role in modulating inflammation in IBD models, we were unable to test therapeutic benefits of pharmacologically activating this channel using currently available compounds, since agonists such as Yoda1 are not cell-type specific and may have off target effects.

RESOURCE AVAILABILITY

Lead contact

Requests for further information and resources should be directed to and will be fulfilled by the lead contact, Ruaidhrí Jackson (ruaidhri_jackson@hms.harvard.edu).

Materials availability

All unique/stable reagents generated in this study are available from the lead contact with a completed materials transfer agreement.

Data and code availability

- This paper analyzes existing, publicly available data, accessible at NCBI at the following accessions: GEO: GSE102962, GEO: GSE153202, GEO: GSE149524, GEO: GSE232789, and SRA: SRP135960. Data are also accessible from the Broad Single Cell Portal at SCP1038.
- All data reported in this paper will be shared by the lead contact upon request.
- This paper does not report any original code.
- Any additional information required to reanalyze the data reported in this paper is available from the lead contact upon request.

ACKNOWLEDGMENTS

This work was supported by the NIH Directors New Innovators Program DP2AI169979 (to R.J.), the Paul Allen Distinguished Investigator Program (to R.J.), the Kenneth Rainin Innovator Award (to R.J. and R.O.), the Crohn's and Colitis of America Foundation Senior Research Award 959859 (to R.J. and Q.R.), the National Science Foundation Graduate Research Fellowship Program DGE2140743 (to L.R.). This work is supported by the Allen Discovery Center program, a Paul G. Allen Frontiers Group advised program of the Paul G. Allen Family Foundation (to B.S.K. and H.H.). H.H. is supported by the National Institute of Diabetes and Digestive and Kidney Diseases (NIDDK) (DK103901, DK134773, and DK141106), NIAMS (AR077183), and the National Institute on Alcohol Abuse and Alcoholism (NIAA) (AA027065) of the NIH. B.S.K. is supported by the National Institute of Arthritis and Musculoskeletal and Skin Diseases (NIAMS) (AR070116, AR077007, and AR080392), NIDDK (DK141106), and the National Institute of Allergy and Infectious Disease (NIAID) (AI167933 and AI167047) of the NIH. We would like to thank Dr. James N. Warnock for the pressure chamber system. We would like to thank Dr. Angel Solis for his comments on the manuscript. We would like to thank Dr. Paula Montero Llopis, Dr. Praju Vikas Anekal, and Dr. Adrienne Wells at MicRoN HMS for help with microscopy. We would also like to thank Dr. Carla J Weinheimer and the Mouse Cardiovascular Phenotyping Core at Washington University in Saint Louis for assistance with rodent treadmill exercises. We would like to thank Dr. Qin Liu for providing the Pirt^{GCamp3} mice.

AUTHOR CONTRIBUTIONS

Z.X., L.R., J.F., H.H., and R.J. initiated the project, designed and conducted experiments, analyzed data, and generated figures. J.F. assisted with immunostaining and behavior assays. Y.Z. helped with patch-clamp recording. Y.L. and A.Z. conducted flow cytometry experiments. H.K. conducted bioinformatic analysis. T.J.H. and N.J.S. helped with CMMC recording. X.H. and K.Z. helped with virus injection. R.O. helped with DSS experiments. Q.R. conducted colon motility assays, while X.Y., F.G., N.A., Z.W., O.V., K.V., H.W., C.B., C.D., L.D., X.M., L.Z., M.H., and R.B. helped with experiments, recording, and/or data interpretation. X.D. donated Pirt^{GCaMP3} and Pirt^{cre} mice. I.M.C., X.D., B.S.K., and N.J.S. helped with comments and suggestions. Z.X., L.R., J.F., H.H., and R.J. wrote the manuscript with contributions from all authors in the interpretation of the data and conclusions of the findings.

DECLARATION OF INTERESTS

H.H. has served as a consultant for Formation Bio and Almirall on topics unrelated to this manuscript, and his lab has received sponsored research

from Triveni Bio. B.S.K. is founder of KliRNA Biotech; he has served as a consultant for 23andMe, ABRAX Japan, AbbVie, Almirall, Amgen, Arcutis Biotherapeutics, Arena Pharmaceuticals, argenx, AstraZeneca, Boehringer Ingelheim, Bristol-Myers Squibb, Cara Therapeutics, Clexio Biosciences, Eli Lilly and Company, Escient Pharmaceuticals, Evommune, Galderma, Genentech, GlaxoSmithKline, Granular Therapeutics, Incyte Corporation, Innovaderm Research, Janssen, Kiniksa, LEO Pharma, Maruho, Novartis, Pfizer, Recens Medical, Regeneron Pharmaceuticals, Sanofi, Septerna, Triveni Bio, Vial, and WebMD; he has stock in ABRAX Japan, KliRNA Biotech, Locus Biosciences, and Recens Medical; he holds a patent for the use of janus kinase 1 (JAK1) inhibitors for chronic pruritus; and he has a patent pending for the use of JAK inhibitors for interstitial cystitis.

STAR★METHODS

Detailed methods are provided in the online version of this paper and include the following:

- KEY RESOURCES TABLE
- EXPERIMENTAL MODEL AND STUDY PARTICIPANT DETAILS
  - Mice
- METHOD DETAILS
  - scRNA-Seq reanalysis
  - Treadmill exercise
  - Whole gut motility assays
  - GI transit
  - Colon transit
  - Food and water consumption measurements
  - Intracolonic injection
  - 6-OHDA treatment
  - Enteric neuron progenitor cell isolation
  - Neuron Differentiation
  - Dissociation of myenteric neurons
  - Single myenteric neuron picking
  - Single cell real-time RT-qPCR
  - Whole-cell patch-clamp recording
  - *Ex vivo* Ca^{2+} imaging
  - CMMC recording
  - Isometric tension recording of colon strips
  - Whole mount microscopy
  - Immunofluorescence
  - Histology
  - Pressure Chamber
  - Ca^{2+} free c-Fos assay
  - Induction of Colitis
  - RNA isolation and RT-PCR
  - LCN2 ELISA
  - Acetylcholine measurements
  - Treatment with Piezo1 pharmacological modulators
  - Isolation of cells from the colon
  - Flow cytometry
- QUANTIFICATION AND STATISTICAL ANALYSIS

SUPPLEMENTAL INFORMATION

Supplemental information can be found online at https://doi.org/10.1016/j.cell.2025.02.031.

Received: May 6, 2024
Revised: November 19, 2024
Accepted: February 25, 2025
Published: March 24, 2025

REFERENCES

1. Fettiplace, R., and Kim, K.X. (2014). The physiology of mechanoelectrical transduction channels in hearing. Physiol. Rev. *94*, 951–986. https://doi.org/10.1152/physrev.00038.2013.
2. Ranade, S.S., Woo, S.H., Dubin, A.E., Moshourab, R.A., Wetzel, C., Petrus, M., Mathur, J., Bégay, V., Coste, B., Mainquist, J., et al. (2014). Piezo2 is the major transducer of mechanical forces for touch sensation in mice. Nature *516*, 121–125. https://doi.org/10.1038/nature13980.
3. Alcaino, C., Farrugia, G., and Beyder, A. (2017). Mechanosensitive piezo channels in the gastrointestinal tract. Curr. Top. Membr. *79*, 219–244. https://doi.org/10.1016/bs.ctm.2016.11.003.
4. Solis, A.G., Bielecki, P., Steach, H.R., Sharma, L., Harman, C.C.D., Yun, S., de Zoete, M.R., Warnock, J.N., To, S.D.F., York, A.G., et al. (2019). Mechanosensation of cyclical force by PIEZO1 is essential for innate immunity. Nature *573*, 69–74. https://doi.org/10.1038/s41586-019-1485-8.
5. Kunze, W.A., and Furness, J.B. (1999). The enteric nervous system and regulation of intestinal motility. Annu. Rev. Physiol. *61*, 117–142. https://doi.org/10.1146/annurev.physiol.61.1.117.
6. Li, Z., Chalazonitis, A., Huang, Y.Y., Mann, J.J., Margolis, K.G., Yang, Q.M., Kim, D.O., Côté, F., Mallet, J., and Gershon, M.D. (2011). Essential roles of enteric neuronal serotonin in gastrointestinal motility and the development/survival of enteric dopaminergic neurons. J. Neurosci. *31*, 8998–9009. https://doi.org/10.1523/JNEUROSCI.6684-10.2011.
7. Furness, J.B. (2000). Types of neurons in the enteric nervous system. J. Auton. Nerv. Syst. *81*, 87–96. https://doi.org/10.1016/s0165-1838(00)00127-2.
8. Jarret, A., Jackson, R., Duizer, C., Healy, M.E., Zhao, J., Rone, J.M., Bielecki, P., Sefik, E., Roulis, M., Rice, T., et al. (2020). Enteric nervous system-derived IL-18 orchestrates mucosal barrier immunity. Cell *180*, 50–63.e12. https://doi.org/10.1016/j.cell.2019.12.016.
9. Heredia, D.J., Dickson, E.J., Bayguinov, P.O., Hennig, G.W., and Smith, T.K. (2009). Localized release of serotonin (5-hydroxytryptamine) by a fecal pellet regulates migrating motor complexes in murine colon. Gastroenterology *136*, 1328–1338. https://doi.org/10.1053/j.gastro.2008.12.010.
10. Heredia, D.J., Grainger, N., McCann, C.J., and Smith, T.K. (2012). Insights from a novel model of slow-transit constipation generated by partial outlet obstruction in the murine large intestine. Am. J. Physiol. Gastrointest. Liver Physiol. *303*, G1004–G1016. https://doi.org/10.1152/ajpgi.00238.2012.
11. Kern, F., Almy, T.P., Abbot, F.K., and Bogdonoff, M.D. (1951). The motility of the distal colon in non-specific ulcerative colitis*. Gastroenterology *19*, 492–503. https://doi.org/10.1016/S0016-5085(19)36411-X.
12. Servin-Vences, M.R., Lam, R.M., Koolen, A., Wang, Y., Saade, D.N., Loud, M., Kacmaz, H., Frausto, S., Zhang, Y., Beyder, A., et al. (2023). PIEZO2 in somatosensory neurons controls gastrointestinal transit. Cell *186*, 3386–3399.e15. https://doi.org/10.1016/j.cell.2023.07.006.
13. Smith-Edwards, K.M., Najjar, S.A., Edwards, B.S., Howard, M.J., Albers, K.M., and Davis, B.M. (2019). Extrinsic primary afferent neurons link visceral pain to colon motility through a spinal reflex in mice. Gastroenterology *157*, 522–536.e2. https://doi.org/10.1053/j.gastro.2019.04.034.
14. Browning, K.N., and Travagli, R.A. (2014). Central nervous system control of gastrointestinal motility and secretion and modulation of gastrointestinal functions. Compr. Physiol. *4*, 1339–1368. https://doi.org/10.1002/cphy.c130055.
15. Spencer, N.J., and Hu, H. (2020). Enteric nervous system: sensory transduction, neural circuits and gastrointestinal motility. Nat. Rev. Gastroenterol. Hepatol. *17*, 338–351. https://doi.org/10.1038/s41575-020-0271-2.
16. Duan, H., Cai, X., Luan, Y., Yang, S., Yang, J., Dong, H., Zeng, H., and Shao, L. (2021). Regulation of the Autonomic Nervous System on Intestine. Front. Physiol. *12*, 700129. https://doi.org/10.3389/fphys.2021.700129.
17. Wood, J.D. (2008). Enteric nervous system: reflexes, pattern generators and motility. Curr. Opin. Gastroenterol. *24*, 149–158. https://doi.org/10.1097/MOG.0b013e3282f56125.
18. Schemann, M. (2005). Control of gastrointestinal motility by the "gut brain"–the enteric nervous system. J. Pediatr. Gastroenterol. Nutr. *41*, S4–S6. https://doi.org/10.1097/01.scs.0000180285.51365.55.
19. Barnes, K.J., Beckett, E.A., Brookes, S.J., Sia, T.C., and Spencer, N.J. (2014). Control of intrinsic pacemaker frequency and velocity of colonic

migrating motor complexes in mouse. Front. Neurosci. *8*, 96. https://doi.org/10.3389/fnins.2014.00096.

20. Najjar, S.A., and Margolis, K.G. (2022). The tactile sensors of the gut. Trends Neurosci. *45*, 173–175. https://doi.org/10.1016/j.tins.2021.12.003.
21. Alcaino, C., Knutson, K.R., Treichel, A.J., Yildiz, G., Strege, P.R., Linden, D.R., Li, J.H., Leiter, A.B., Szurszewski, J.H., Farrugia, G., et al. (2018). A population of gut epithelial enterochromaffin cells is mechanosensitive and requires Piezo2 to convert force into serotonin release. Proc. Natl. Acad. Sci. USA *115*, E7632–E7641. https://doi.org/10.1073/pnas.1804938115.
22. Min, S., Oh, Y., Verma, P., Whitehead, S.C., Yapici, N., Van Vactor, D., Suh, G.S., and Liberles, S. (2021). Control of feeding by Piezo-mediated gut mechanosensation in Drosophila. eLife *10*, e63049. https://doi.org/10.7554/eLife.63049.
23. Sugisawa, E., Takayama, Y., Takemura, N., Kondo, T., Hatakeyama, S., Kumagai, Y., Sunagawa, M., Tominaga, M., and Maruyama, K. (2020). RNA Sensing by Gut Piezo1 Is Essential for Systemic Serotonin Synthesis. Cell *182*, 609–624.e21. https://doi.org/10.1016/j.cell.2020.06.022.
24. Zhao, Y., Liu, Y., Tao, T., Zhang, J., Guo, W., Deng, H., Han, M., Mo, H., Tong, X., Lin, S., et al. (2024). Gastric mechanosensitive channel Piezo1 regulates ghrelin production and food intake. Nat. Metab. *6*, 458–472. https://doi.org/10.1038/s42255-024-00995-z.
25. Drokhlyansky, E., Smillie, C.S., Van Wittenberghe, N., Ericsson, M., Griffin, G.K., Eraslan, G., Dionne, D., Cuoco, M.S., Goder-Reiser, M.N., Sharova, T., et al. (2020). The human and mouse enteric nervous system at single-cell resolution. Cell *182*, 1606–1622.e23. https://doi.org/10.1016/j.cell.2020.08.003.
26. Morarach, K., Mikhailova, A., Knoflach, V., Memic, F., Kumar, R., Li, W., Ernfors, P., and Marklund, U. (2021). Diversification of molecularly defined myenteric neuron classes revealed by single-cell RNA sequencing. Nat. Neurosci. *24*, 34–46. https://doi.org/10.1038/s41593-020-00736-x.
27. May-Zhang, A.A., Tycksen, E., Southard-Smith, A.N., Deal, K.K., Benthal, J.T., Buehler, D.P., Adam, M., Simmons, A.J., Monaghan, J.R., Matlock, B.K., et al. (2021). Combinatorial transcriptional profiling of mouse and human enteric neurons identifies shared and disparate subtypes in situ. Gastroenterology *160*, 755–770.e26. https://doi.org/10.1053/j.gastro.2020.09.032.
28. Ranade, S.S., Qiu, Z., Woo, S.H., Hur, S.S., Murthy, S.E., Cahalan, S.M., Xu, J., Mathur, J., Bandell, M., Coste, B., et al. (2014). Piezo1, a mechanically activated ion channel, is required for vascular development in mice. Proc. Natl. Acad. Sci. USA *111*, 10347–10352. https://doi.org/10.1073/pnas.1409233111.
29. Sharkey, K.A., Parr, E.J., and Keenan, C.M. (1999). Immediate-early gene expression in the inferior mesenteric ganglion and colonic myenteric plexus of the guinea pig. J. Neurosci. *19*, 2755–2764. https://doi.org/10.1523/JNEUROSCI.19-07-02755.1999.
30. Fung, C., Koussoulas, K., Unterweger, P., Allen, A.M., Bornstein, J.C., and Foong, J.P.P. (2018). Cholinergic submucosal neurons display increased excitability following in vivo cholera toxin exposure in mouse ileum. Front. Physiol. *9*, 260. https://doi.org/10.3389/fphys.2018.00260.
31. West, A.E., and Greenberg, M.E. (2011). Neuronal activity-regulated gene transcription in synapse development and cognitive function. Cold Spring Harb. Perspect. Biol. *3*, a005744. https://doi.org/10.1101/cshperspect.a005744.
32. Ruest, L.-B., Dager, M., Yanagisawa, H., Charité, J., Hammer, R.E., Olson, E.N., Yanagisawa, M., and Clouthier, D.E. (2003). Dhand-cre transgenic mice reveal specific potential functions of dHAND during craniofacial development. Dev. Biol. *257*, 263–277. https://doi.org/10.1016/S0012-1606(03)00068-X.
33. Gabanyi, I., Muller, P.A., Feighery, L., Oliveira, T.Y., Costa-Pinto, F.A., and Mucida, D. (2016). Neuro-immune interactions drive tissue programming in intestinal macrophages. Cell *164*, 378–391. https://doi.org/10.1016/j.cell.2015.12.023.
34. Hendershot, T.J., Liu, H., Sarkar, A.A., Giovannucci, D.R., Clouthier, D.E., Abe, M., and Howard, M.J. (2007). Expression of Hand2 is sufficient for neurogenesis and cell type-specific gene expression in the enteric nervous system. Dev. Dyn. *236*, 93–105. https://doi.org/10.1002/dvdy.20989.
35. Hibberd, T.J., Feng, J., Luo, J., Yang, P., Samineni, V.K., Gereau, R.W.t., Kelley, N., Hu, H., and Spencer, N.J. (2018). Optogenetic induction of colonic motility in mice. Gastroenterology *155*, 514–528.e6. https://doi.org/10.1053/j.gastro.2018.05.029.
36. Ray, R.S., Corcoran, A.E., Brust, R.D., Kim, J.C., Richerson, G.B., Nattie, E., and Dymecki, S.M. (2011). Impaired respiratory and body temperature control upon acute serotonergic neuron inhibition. Science *333*, 637–642. https://doi.org/10.1126/science.1205295.
37. Zeisel, A., Hochgerner, H., Lönnerberg, P., Johnsson, A., Memic, F., van der Zwan, J., Häring, M., Braun, E., Borm, L.E., La Manno, G., et al. (2018). Molecular architecture of the mouse nervous system. Cell *174*, 999–1014.e22. https://doi.org/10.1016/j.cell.2018.06.021.
38. Hockley, J.R.F., Taylor, T.S., Callejo, G., Wilbrey, A.L., Gutteridge, A., Bach, K., Winchester, W.J., Bulmer, D.C., McMurray, G., and Smith, E.S.J. (2019). Single-cell RNAseq reveals seven classes of colonic sensory neuron. Gut *68*, 633–644. https://doi.org/10.1136/gutjnl-2017-315631.
39. Billipp, T.E., Fung, C., Webeck, L.M., Sargent, D.B., Gologorsky, M.B., Chen, Z., McDaniel, M.M., Kasal, D.N., McGinty, J.W., Barrow, K.A., et al. (2024). Tuft cell-derived acetylcholine promotes epithelial chloride secretion and intestinal helminth clearance. Immunity *57*, 1243–1259.e8. https://doi.org/10.1016/j.immuni.2024.03.023.
40. Ndjim, M., Gasmi, I., Herbert, F., Joséphine, C., Bas, J., Lamrani, A., Coutry, N., Henry, S., Zimmermann, V.S., Dardalhon, V., et al. (2024). Tuft cell acetylcholine is released into the gut lumen to promote anti-helminth immunity. Immunity *57*, 1260–1273.e7. https://doi.org/10.1016/j.immuni.2024.04.018.
41. Haber, A.L., Biton, M., Rogel, N., Herbst, R.H., Shekhar, K., Smillie, C., Burgin, G., Delorey, T.M., Howitt, M.R., Katz, Y., et al. (2017). A single-cell survey of the small intestinal epithelium. Nature *551*, 333–339. https://doi.org/10.1038/nature24489.
42. Chai, X.Y., Diwakarla, S., Pustovit, R.V., McQuade, R.M., Di Natale, M., Ermine, C.M., Parish, C.L., Finkelstein, D.I., and Furness, J.B. (2020). Investigation of nerve pathways mediating colorectal dysfunction in Parkinson's disease model produced by lesion of nigrostriatal dopaminergic neurons. Neurogastroenterol. Motil. *32*, e13893. https://doi.org/10.1111/nmo.13893.
43. Bassotti, G., Antonelli, E., Villanacci, V., Salemme, M., Coppola, M., and Annese, V. (2014). Gastrointestinal motility disorders in inflammatory bowel diseases. World J. Gastroenterol. *20*, 37–44. https://doi.org/10.3748/wjg.v20.i1.37.
44. Zheng, W., Song, H., Luo, Z., Wu, H., Chen, L., Wang, Y., Cui, H., Zhang, Y., Wang, B., Li, W., et al. (2021). Acetylcholine ameliorates colitis by promoting IL-10 secretion of monocytic myeloid-derived suppressor cells through the nAChR/ERK pathway. Proc. Natl. Acad. Sci. USA *118*, e2017762118. https://doi.org/10.1073/pnas.2017762118.
45. Xie, Z., Feng, J., Hibberd, T.J., Chen, B.N., Zhao, Y., Zang, K., Hu, X., Yang, X., Chen, L., Brookes, S.J., et al. (2023). Piezo2 channels expressed by colon-innervating TRPV1-lineage neurons mediate visceral mechanical hypersensitivity. Neuron *111*, 526–538.e4. https://doi.org/10.1016/j.neuron.2022.11.015.
46. Mercado-Perez, A., and Beyder, A. (2022). Gut feelings: mechanosensing in the gastrointestinal tract. Nat. Rev. Gastroenterol. Hepatol. *19*, 283–296. https://doi.org/10.1038/s41575-021-00561-y.
47. Fedele, L., and Brand, T. (2020). The intrinsic cardiac nervous system and its role in cardiac pacemaking and conduction. J. Cardiovasc. Dev. Dis. *7*, 54. https://doi.org/10.3390/jcdd7040054.
48. Freem, L.J., Escot, S., Tannahill, D., Druckenbrod, N.R., Thapar, N., and Burns, A.J. (2010). The intrinsic innervation of the lung is derived from neural crest cells as shown by optical projection tomography in Wnt1-Cre;YFP

reporter mice. J. Anat. *217*, 651–664. https://doi.org/10.1111/j.1469-7580.2010.01295.x.

49. Fang, F., Liu, Y., Xiong, Y., Li, X., Li, G., Jiang, Y., Hou, X., and Song, J. (2023). Slowed intestinal transit induced by less mucus in intestinal goblet cell Piezo1-deficient mice through impaired epithelial homeostasis. Int. J. Mol. Sci. *24*, 14377. https://doi.org/10.3390/ijms241814377.
50. Aykut, B., Chen, R., Kim, J.I., Wu, D., Shadaloey, S.A.A., Abengozar, R., Preiss, P., Saxena, A., Pushalkar, S., Leinwand, J., et al. (2020). Targeting Piezo1 unleashes innate immunity against cancer and infectious disease. Sci. Immunol. *5*, eabb5168. https://doi.org/10.1126/sciimmunol.abb5168.
51. Atcha, H., Jairaman, A., Holt, J.R., Meli, V.S., Nagalla, R.R., Veerasubramanian, P.K., Brumm, K.T., Lim, H.E., Othy, S., Cahalan, M.D., et al. (2021). Mechanically activated ion channel Piezo1 modulates macrophage polarization and stiffness sensing. Nat. Commun. *12*, 3256. https://doi.org/10.1038/s41467-021-23482-5.
52. Du, H., Bartleson, J.M., Butenko, S., Alonso, V., Liu, W.F., Winer, D.A., and Butte, M.J. (2023). Tuning immunity through tissue mechanotransduction. Nat. Rev. Immunol. *23*, 174–188. https://doi.org/10.1038/s41577-022-00761-w.
53. Korsunsky, I., Millard, N., Fan, J., Slowikowski, K., Zhang, F., Wei, K., Baglaenko, Y., Brenner, M., Loh, P.R., and Raychaudhuri, S. (2019). Fast, sensitive and accurate integration of single-cell data with Harmony. Nat. Methods *16*, 1289–1296. https://doi.org/10.1038/s41592-019-0619-0.
54. Alquicira-Hernandez, J., and Powell, J.E. (2021). Nebulosa recovers single-cell gene expression signals by kernel density estimation. Bioinformatics *37*, 2485–2487. https://doi.org/10.1093/bioinformatics/btab003.
55. Garnier, S., Ross, N., Rudis, R., Camargo, A.P., Sciaini, M., and Scherer, C.. viridis(Lite) - Colorblind-Friendly Color Maps for R. viridis package version 0.6.5. https://sjmgarnier.github.io/viridis/.
56. Wickham, H. (2016). ggplot2: Elegant Graphics for Data Analysis (New York: Springer-Verlag).
57. Wickham, H. (2007). Reshaping Data with the reshape Package. J. Stat. Soft. *21*, 1–20. http://www.jstatsoft.org/v21/12/.
58. Gu, Z., Eils, R., and Schlesner, M. (2016). Complex heatmaps reveal patterns and correlations in multidimensional genomic data. Bioinform *32*, 2847–2849. https://doi.org/10.1093/bioinformatics/btw313.
59. Gu, Z., Gu, L., Eils, R., Schlesner, M., and Brors, B. (2014). circlize implements and enhances circular visualization in R. Bioinform. *30*, 2811–2812.
60. Hao, Y., Stuart, T., Kowalski, M.H., Choudhary, S., Hoffman, P., Hartman, A., Srivastava, A., Molla, G., Madad, S., Fernandez-Granda, C., et al. (2024). Dictionary learning for integrative, multimodal and scalable single-cell analysis. Nat. Biotechnol. *42*, 293–304. https://doi.org/10.1038/s41587-023-01767-y.
61. Pedersen, T. (2024). patchwork: The Composer of Plots. R package version 1.3.0.9000. https://patchwork.data-imaginist.com.
62. Sivori, M., Dempsey, B., Chettouh, Z., Boismoreau, F., Ayerdi, M., Eymael, A.N., Baulande, S., Lameiras, S., Coulpier, F., Delattre, O., et al. (2024). The Pelvic Organs Receive no Parasympathetic Innervation (ELife Sciences Publications, Ltd).
63. Pearson, K. (1901). LIII. On lines and planes of closest fit to systems of points in space. Lond. Edinb. Dublin Philos. Mag. J. Sci. *2*, 559–572. https://doi.org/10.1080/14786440109462720.
64. McInnes, L.A., Healy, J., and Melville, J. (2018). UMAP: Uniform Manifold Approximation and Projection. Preprint at arXiv. https://doi.org/10.48550/arXiv.1802.03426.
65. Xie, Z., Feng, J., Cai, T., McCarthy, R., Eschbach, M.D., 2nd, Wang, Y., Zhao, Y., Yi, Z., Zang, K., Yuan, Y., et al. (2022). Estrogen metabolites increase nociceptor hyperactivity in a mouse model of uterine pain. JCI Insight *7*, e149107. https://doi.org/10.1172/jci.insight.149107.
66. Schipke, K.J., To, S.D.F., and Warnock, J.N. (2011). Design of a cyclic pressure bioreactor for the ex vivo study of aortic heart valves. Jove, e3316. https://doi.org/10.3791/3316.
67. Laidlaw, B.J., Lu, Y., Amezquita, R.A., Weinstein, J.S., Vander Heiden, J.A., Gupta, N.T., Kleinstein, S.H., Kaech, S.M., and Craft, J. (2017). Interleukin-10 from CD4(+) follicular regulatory T cells promotes the germinal center response. Sci. Immunol. *2*, eaan4767. https://doi.org/10.1126/sciimmunol.aan4767.

STAR★METHODS

KEY RESOURCES TABLE

REAGENT or RESOURCE	SOURCE	IDENTIFIER
Antibodies		
c-Fos	Cell Signaling Technology	Cat# 2250S; RRID:AB_2247211
HuC/HuD	ThermoFisher Scientific	Cat#16A11;RRID:AB_221448
ChAT	Sigma Aldrich	Cat# AB144P; RRID: AB_2079751
NOS	Sigma Aldrich	Cat# AB1529; RRID: AB_90743
RFP	Abcam	Cat# ab185921; RRID: AB_2934052
DsRed	Takara Bio	Cat# 632496; RRID: AB_10013483
GFP	Aves Labs	Cat# GFP-1020; RRID: AB_10000240
CD31	BD Biosciences	Cat# 550274; RRID: AB_393571
F4/80	BioLegend	Cat# 123102; RRID: AB_893504
TUBB3	Biolegend	Cat# 801210; RRID: AB_2686931
Cyanine3 Streptavidin	Biolegend	Cat# 405215
Alexa 488	Invitrogen	Cat# A-11008;
CD11b	Biolegend	Cat# 101219; RRID: AB_493545
Ly6C-FITC (clone HK1.4)	Biolegend	RRID: AB_1186135
MHCII-PE (clone M5/114.15.2)	Biolegend	RRID: AB_313323
CD64-APC (clone x54-5/7.1)	Biolegend	RRID: AB_2910296
SiglecF-PE-cy7 (clone S17007L)	Biolegend	RRID: AB_2904295
EpCam-APC-cy7 (clone G8.8)	Biolegend	RRID: AB_1501158
Ly6G-BV421 (clone 1A8)	Biolegend	RRID: AB_2565880
CD11c-BV605 (clone N418)	Biolegend	RRID: AB_11204262
CD11b-BV711 (clone M1/70)	Biolegend	RRID: AB_2563310
CD45-FITC (clone 30-F11)	Biolegend	RRID: AB_312973
NK.1-PE (clone PK136)	Biolegend	RRID: AB_313395
CD8-APC (clone 53-6.7)	Biolegend	RRID: AB_312751
B220-BV421 (clone RA3-6B2)	Biolegend	RRID: AB_11203535
TCRβ-BV605 (clone H57-597)	Biolegend	RRID: AB_2629563
CD4-BV711 (clone RM4-5)	Biolegend	RRID: AB_2562607
CD11b-PE-y7 (clone M1/70)	Biolegend	RRID: AB_312791
CD16/32 (clone 93)	Biolegend	RRID: AB_2819783
CD45-BV395 (clone 30-F11)	BD Biosceinces	RRID: AB_394606
Live/Dead BV510	BD Biosceinces	Cat# 564406; RRID: AB_2869572
Bacterial and virus strains		
rAAV-ChAT-Cre-WPRE-hGH-pA	BrainVTA	Cat# PT-0607
rAAV-ChAT-GFP-WPRE-hGH-pA	BrainVTA	Cat# PT-1722
Chemicals, peptides, and recombinant proteins		
Carmine Red	Sigma Aldrich	Cat# C1022
FITC dextran	Sigma Aldrich	Cat# 46945
6-OHDA	Sigma Aldrich	Cat# H4381-100MG
Dispase	Stem Cell Tech	Cat# 07923
collagenase type IV	Stem Cell tech	Cat# 07909
Neurocult Basal Medium	Stem Cell Tech	Cat#05700
Neurocult Proliferation Medium	Stem Cell Tech	Cat#05701
EGF	Stem Cell Tech	Cat#78006
bFGF	Stem Cell Tech	Cat#78003

(*Continued on next page*)

Continued

REAGENT or RESOURCE	SOURCE	IDENTIFIER
Heparin Solution	Stem Cell Tech	Cat#07980
Accutase	Stem Cell Tech	Cat#07922
Neurobasal Plus	Thermo Fisher	Cat# A3582901
B-27	Thermo Fisher	Cat#21103049
PenStrep	Sigma Aldrich	Cat# P4333
Single Cell Lysis/DNase I solution	Invitrogen	Cat#4458237
Glycoblue	Thermo Fisher	Cat# AM9516
Maxima H Minus Reverse Transcriptase	Thermo Fisher	Cat# EP0751
Oligo DTs	Thermo Fisher	Cat# SO132
RNAse OUT	Fisher Sci	Cat#1077019
SYBR Green Supermix	Thermo Fisher	Cat# 4309155
Yoda	Sigma	Cat# SML1558
GsMTx-4	Abcam	Cat#ab141871
Glial Derived Neurotrophic factor	Thermo Fisher	Cat#4504410UG
Dako serum free protein block	Aligent	Cat#X0909
Carnoy's fixative	VWR	Cat#101205-852
DSS	TdB Labs	Cat# 9011-18-1
RT buffer	Thermo Fisher	Cat#EP0751
Critical commercial assays		
Mouse LCN2/NGAL Duoset ELISA	R&D Systems	Cat# DY1857
Choline/Acetylcholine Assay Kit	Abcam	Cat# ab65345
Single Cell-to-CT™ real-time RT-qPCR Kit	Invitrogen	Cat# 4458237
Experimental models: Organisms/strains		
Mouse: Piezo1^{TdTomato}: B6;129-*Piezo1*$^{tm1.1Apat}$/J	The Jackson Laboratory	Cat# 029214
Mouse: Piezo1$^{fl/fl}$: B6.Cg-*Piezo1*$^{tm2.1Apat}$/J	The Jackson Laboratory	Cat# 029213
Mouse: Piezo1^{Flpo}	Generated by Hu lab	N/A
Mouse: Piezo2$^{fl/fl}$: B6(SJL)-*Piezo2*$^{tm2.2Apat}$/J	The Jackson Laboratory	Cat#027720
Mouse: Pirt^{cre}	Gift from Xingzhong Dong Lab	N/A
Mouse: Hand2^{cre}	Gift from David E. Clouthier Lab	N/A
Mouse: ChAT^{cre}: B6.129S-*Chat*$^{tm1(cre)Lowl}$/MwarJ	The Jackson Laboratory	Cat#031661
Mouse: VIP^{cre}: B6J.Cg-*Vip*$^{tm1(cre)Zjh}$/AreckJ	The Jackson Laboratory	Cat#031628
Mouse: Nos1$^{ERT2\text{-}cre}$: B6;129S-*Nos1*$^{tm1.1(cre/ERT2)Zjh}$/J	The Jackson Laboratory	Cat#014541
Mouse: Plp1$^{ERT2\text{-}cre}$: B6.Cg-Tg(Plp1-cre/ERT)3Pop/J	The Jackson Laboratory	Cat#005975
Mouse:ReaChR-mCitrine: B6;129S-*Gt(ROSA)26Sor*$^{tm2.1Ksvo}$/J	The Jackson Laboratory	Cat#024846
Mouse: RC::FPDi B6;129S6-*Gt(ROSA)26Sor*$^{tm9(CAG\text{-}mCherry,\text{-}CHRM4^{*})Dym}$/J	The Jackson Laboratory	Cat#029040
Mouse: Pirt^{GCamp3}	Gift from Xingzhong Dong Lab	N/A
Mouse: C57BL/6J	The Jackson Laboratory	Cat#000664
Oligonucleotides		
Piezo1	TaqMan assay	Mm01241549_m1
Piezo2	TaqMan assay	Mm01262433_m1
ChAT	TaqMan assay	Mm01221880_m1
Nos1	TaqMan assay	Mm01208059_m1
Elavl3	TaqMan assay	Mm01151962_m1
Gapdh	TaqMan assay	Mm99999915_g1
Primer for generic cre Forward: TTCCCGCAGAACCTGAAGA TGTTCG; Reverse:GCCAGATTACGTATATCCTGGCAGC	Millipore sigma	N/A
Primer for Piezo1-FlpO: Forward: GCTGTGCCAGGACATCT TCTTGGTG Reverse: ACAGGATGTCGAACTGGCTCATCAC	JAX protocol; Ordered from Millipore sigma	N/A

(*Continued on next page*)

Continued

REAGENT or RESOURCE	SOURCE	IDENTIFIER
Primer for ReaChR-mCitrine: Mutant: CCA GGC GGG CCA TTT ACC GTA AG Common: AAA GTC GCT CTG AGT TGT TAT Wild type: GGA GCG GGA GAA ATG GAT ATG	JAX protocol; Ordered from Millipore sigma	N/A
Primers for RC::FPDi: Mutant Forward: AGT AAG CTT GGG CTG CAG GT; Mutant Reverse: CAT TGA CAG GTG TGA AGT TGG; Wild Type Forward: AAG GGA GCT GCA GTG GAG TA; Wild Type Reverse: CAG GAC AAC GCC CAC ACA	JAX protocol; Ordered from Millipore sigma	N/A
Software and algorithms		
GraphPad Prism	GraphPad	https://www.graphpad.com/features
FlowJo	FlowJo	https://www.flowjo.com/solutions/flowjo/downloads
ImageJ	FIJI	https://imagej.net/software/fiji/
R version v4.3.3	R Foundation for Statistical Computing, Vienna, Austria.	https://cran.r-project.org/
RStudio Desktop v2023.12.1.402	RStudio, PBC, Boston, MA, USA.	https://posit.co/downloads/
Pop!_OS 22.04 LTS Linux GNU (64 bit)	System76, Denver, CO, USA.	https://pop.system76.com/
Illustrator CS6	Adobe	https://www.adobe.com/products/illustrator.html
EthoVision XT 13	Noldus	RRID: SCR_000441
pClamp	Molecular Devices	RRID: SCR_011323
LabChart 8	ADInstruments	https://www.adinstruments.com/products/labchart
LAS X	Leica Microsystems	https://www.leica-microsystems.com/products/microscope-software/p/leica-las-x-ls/
Harmony v1.2.1	Korsunsky et al.[53]	https://github.com/immunogenomics/harmony
Nebulosa v1.14.0	Alquicira-Hernandez et al.[54]	https://github.com/powellgenomicslab/Nebulosa
viridis v0.6.5	Garnier et al.[55]	https://sjmgarnier.github.io/viridis/
extrafont v0.19	https://www.rdocumentation.org/packages/extrafont/versions/0.19	https://github.com/wch/extrafont
ggplot2 v3.5.0	Wickham[56]	https://github.com/tidyverse/ggplot2
ggtext v0.1.2	https://wilkelab.org/ggtext/articles/introduction.html	https://github.com/wilkelab/ggtext
reshape2 v1.4.4	Wickham[57]	https://github.com/cran/reshape2
ComplexHeatmap v2.20.0	Gu et al.[58]	https://github.com/jokergoo/ComplexHeatmap
circlize 0.4.16	Gu et al.[59]	https://github.com/jokergoo/circlize
Seurat single cell genomics toolkit v5.0.3	Hao et al.[60]	https://github.com/satijalab/seurat
patchwork v1.2.0	Pedersen[61]	https://github.com/thomasp85/patchwork

EXPERIMENTAL MODEL AND STUDY PARTICIPANT DETAILS

Mice

All animal experiments used in this study were approved by the Animal Studies Committee at Icahn School of Medicine at Mount Sinai, Washington University in Saint Louis, or Harvard Medical School. For visualization of endogenous Piezo1 protein, a tdTomato-Piezo1 c-terminus fusion reporter mouse (Jax# 029214) was used. For deletion of Piezo1 (Jax# 029213) and Piezo2 (Jax# 027720) in the enteric nervous system, mice were crossed to Hand2-cre mice generated and generously gifted to us by Dr. David E. Clouthier.[32] For conditional deletion in specific neuron subtypes mice were bread to cre expressing strains from Jackson

Laboratories: ChAT^{cre} (Jax# 031661) to target cholinergic neurons, VIP^{cre} (Jax #031628) for deletion in vasoactive intestinal polypeptide expressing neurons, Nos1$^{ERT2\text{-}cre}$ (Jax# 014541) for deletion in neuronal nitric oxide synthase 1 expressing neruons and PLP1$^{ERT2\text{-}cre}$ (Jax #005975) to target enteric glial cells. RC::FPDi (Jax #029040), and ReaChR-mCitrine (Jax# 024846) mice were obtained from the Jackson Laboratory (Bar Harbor, ME, USA). To generate the Piezo1^{flpo} mouse line, a target vector containing the P2A-FlpO was inserted after the exon 51 of the gene Piezo1 by homologous recombination using CRISPR/Cas9. Both male and female mice 7-12 weeks old were used for all experiments. 4-weeks old mice were used for virus injection. Mice were used in behavior experiments at about 8 weeks of age. Animals that were compared between groups in single experiments were bred to generate littermates and were cohoused for all experiments to minimize confounding affects for the intestinal microbiota. All animals were maintained in a specific pathogen free barrier facility. All motility studies were conducted during the animal's light cycle. Animal experimentation was conducted in compliance with Icahn School of Medicine at Mount Sinai Institutional Animal Care and Use Committee protocols, Washington University in Saint Louis Institutional Animal Care and Use Committee protocols, or Harvard Medical School Institutional Animal Care and Use Committee protocols.

METHOD DETAILS

scRNA-Seq reanalysis

Processed 10x scRNA-seq data files from 7 different neuronal single cell RNA-seq studies were downloaded from their corresponding repositories.[25–27,37,38,41,62] Data were reanalyzed using the Seurat V5 single cell genomics toolkit.[60] Raw count matrices corresponding were combined into a single Seurat object and, where necessary, count data were merged using the JoinLayers() function. Data were normalized for dimensionality reduction using SCTransform with default settings and principal component analysis,[63] was performed using the Seurat RunPCA() function with npcs = 100. For the integrated dataset, contaminating non-neuronal populations were iteratively filtered out based on gene expression and cell clustering. Integration was performed using harmony (https://github.com/immunogenomics/harmony[53]). Uniform manifold approximation[64] and projection as performed using the Seurat RunUMAP() function with reduction = "harmony". Log-normalized counts for other analyses and visualization were generated using the Seurat NormalizeData() function with normalization.method = "LogNormalize", scale.factor = 10000, using the raw count data as input. Cluster-level average log-normalized expression counts were generated using the Seurat AverageExpression() function. Where indicated, cluster-level average log-normalized counts were scaled using the base R scale() function. The following R packages were used for analysis and visualization: Seurat v5.0.3, harmony v1.2.1, nebulosa v1.14.0, viridis v0.6.5, ScCustomize v2.1.2, extrafont v0.19, ggplot2 v3.5.0, ggtext v0.1.2, reshape2 v1.4.4, patchwork v1.2.0, ComplexHeatmap v2.20.0, and circlize 0.4.16. Sequencing data reanalyses were performed using R version v4.3.3 and RStudio Desktop v2023.12.1.402 on a Pop!_OS 22.04 LTS Linux GNU (64 bit) system.

Treadmill exercise

Mice were acclimated to treadmill running over 5 days (from day 1 to day 5) at a speed of 12 m/min for 20 minutes each session. Following acclimation phase, mice were granted 2 days of rest. On day 8, mice were randomized into different groups and motility measures. Mice were subjected to treadmill exercise 30 min following gavaging FITC-dextran. Each group of mice then underwent different exercise durations, including 0, 5, 10, and 20 minutes. 90 minutes after gavaging FITC-dextran, the mice were sacrificed to assess GI transit.

Whole gut motility assays

Mice were gavaged with 300 μL of 6% carmine red (Sigma Aldrich#, C1022) in 0.5% methyl cellulose. The time for the appearance of the first red fecal pellet was recorded. All experiments were conducted at the same time of day.

GI transit

GI transit was evaluated following the gavage of FITC-labeled dextran in PBS. In brief, each mouse was injected with 100 mL FITC-Dextran (5 mg/ml) by oral gavage and sacrificed 90 min later to remove the whole GI tract which was divided into 15 segments. The luminal contents in the stomach (Segment #1), small intestine segments (Segments #2–#11), cecum (Segment #12), and colon segments (Segments #13–#15) were flushed with 1 ml Krebs solution and centrifuged at 13,000g for 10 min. The FITC fluorescence intensity of the supernatant in each segment was measured at 494 nm (absorption) / 521 nm (emission) wavelength. The geometric center (GC) was calculated using the formula: GC = Σ (% of total fluorescent signal per segment × segment number) / 100.

Colon transit

Colon transit was assessed as the time required to expel a glass bead (3 mm in diameter) inserted 3 cm into the rectum. In brief, following over-night fasting only with access to water, mice were anesthetized with inhalation of isoflurane, and a 3-mm glass bead was inserted through the anus and pushed 3 cm towards the oral by a customized needle with a silicon cannula (3 mm in diameter). The needle was then withdrawn lightly. The time required to eject the bead was measured as an estimate of colonic motility.

Food and water consumption measurements

Two to five mice were placed in each cage, and the food and water consumed by each cage was recorded daily for 3 days. The average consumption of food and water per mouse every 24 hours was reported.

Intracolonic injection

Intracolonic injection of AAV was performed as previously described.[45] In brief, mice were anesthetized with inhalation of isoflurane, and artificial tears were used to prevent dehydration of the eyes. After shaving and sterilization of the abdomen mice were placed on a sterile surgical pad and covered with a sterile surgical drape. After the colon tissue was exposed by making a midline incision through the abdominal wall, 2 μL of virus (500 nL*4 sites) was injected at a flow rate of 100 nL/minute and the needle was left in place for 5 minutes. Following injection, the abdominal wall and the skin were closed using surgical sutures before antibiotic ointment was applied to the closed surgical site. Behavioral data and tissues were collected for analysis 4 weeks after injections.

6-OHDA treatment

6-OHDA from Sigma (Cat # H4381-100MG) was dissolved in 0.01% ascorbic acid and administered via intraperitoneal injection at 150 mg/kg body weight for two consecutive days. The mice were allowed to recover for 5 days after the last injection before performing experiments. Sympathetic ablation was confirmed by TH staining.

Enteric neuron progenitor cell isolation

Small intestines from 6 weeks old male or female WT C57BL/6J (Jax# 000664) were flushed with cold HBSS and cut into 2-4 cm pieces. Colon pieces were placed on a pipette tip and the myenteric plexus and longitudinal muscle layer was separated from the mucosa using a wet Q-tip and stored in cold HBSS. To digest, HBSS was aspirated and 37°C dispase (StemCell Tech# 07923) was added to tissue for 12 minutes in 37°C water bath. The tissue was then centrifuged at 200 rcf for 5 minutes at 4°C and dispase was aspirated. All spins were at 200 rcf at 4°C for 5 minutes. Then 37°C collagenase type IV (Sigma) digestion medium was added and incubated for 10 minutes in 37°C water bath. The tissue was spun again collagenase was aspirated. The tissue was washed 2X with 20 mL cold HBSS. In a 50 mL tube, 10 mL of prewarmed 37°C 0.05% Trypsin-EDTA diluted in HBSS was added to tissue for 5 minutes while shaking in 37°C water bath. The trypsin is then neutralized in 13 mL of cold digestion neutralizing medium (DMEM/F12 [10% FBS]) and spun down. After aspirating, the tissue was vigorously triturated with a 1000 mL pipette, and 20 mL HBSS was added and spun. The pellet was resuspended in 20 mL HBSS and filtered into new 50 mL tube using a 70 μM filter. The cells were spun and supernatant was removed. The cells were then resuspended in 1 mL of proliferation media (44.3 mL Neurocult Basal Medium [Stemcell Tech# 05700], 5 mL Neurocult Proliferation Medium [Stemcell Tech# 05701], 100 μL 10 ug/mL EGF [Stemcell Tech#. 78006], 100 μL 10 μg/mL bFGF [Stemcell Tech#. 78003], 50 μL Heparin Solution [Stemcell Tech# 07980] and 500 μL antibiotic/antimycotic). Cells were then counted and then equally distributed in 500 μL proliferation media in non-treated 24 well plates where they generated into neurospheres.

Neuron Differentiation

After 5-7 days, neurospheres were collected and spun at 4°C at 90 rcf for 1 minute. Supernatant was aspirated and 800 μL of Accutase (Stemcell Tech # 07922) was added and incubated for 15 minutes at 37°C. Then Accutase was neutralized with 1.6 mL differentiation media (47.5mL Neurobasal Plus [ThermoFisher # A3582901], 1 mL B27, 500 μL FBS-C, 500 μL L-glutamine, 50 μL Glial Derived Neurotrophic factor, and 500 μL antibiotic/antimycotic) and spun at 210 rcf for 5 minutes. Supernatant was aspirated and 1 mL of differentiation media was added to the pellet to resuspend and cells were counted. Cells were plated on Conrning Matrigel coated 24-well glass bottom plates for imaging with 500 μL differentiation media that was changed every 3 days for 1-2 weeks.

Dissociation of myenteric neurons

Colon tissues were collected after mice were euthanized by CO2 asphyxiation and placed into ice-cold carbogen-bubbled (95% O2, 5% CO2) Krebs solution containing (in mM): 118 NaCl, 4.6 KCl, 1.3 NaH2PO4, 1.2 MgSO4, 25 NaHCO3, 11 glucose, and 2.5 CaCl2. The whole-mount myenteric plexus preparations were separated from the underlying circular muscle and washed 3 times with Krebs solution to remove contamination. Segments of whole-mount myenteric plexus were then placed into a digestion solution containing 13 mg type 2 collagenase and 3 mg BSA in 10 ml carbogen-bubbled Krebs solution for 60 min at 37 °C. After digestion, tissues were collected by centrifugation at 356g for 5 min and then digested in 0.05% trypsin solution at 37 °C for 7 min with shaking. Dissociated cells were collected by centrifugation (5 min, 356g) and incubated in neurobasal-A culture medium containing 2% B-27 supplement (Thermo Fisher# 21103049), 100 U/mL penicillin plus 100 μg/mL streptomycin (Sigma-Aldrich# P4333). Cells were kept in a humidified incubator at 37 °C with 5% CO2.

Single myenteric neuron picking

Myenteric neurons were isolated from the colon preparations of reporter mice, and then purified with a 15% BSA density gradient column. A Nikon Eclipse TE200-S microscope was used to visually identify individual tdTomato-labeled myenteric neurons which were picked using a micromanipulator (Sutter Instrument). Individual myenteric neurons were drawn into the tip of a pulled glass electrode filled with HBSS using negative pressure and were transferred to a PCR tube containing 10 μL of Single Cell Lysis/DNase I solution (Invitrogen# 4458237) and were processed Single-cell real-time RT-qPCR according to the manual.

Single cell real-time RT-qPCR

Single-cell real-time RT-qPCR was performed as described[65] using the Invitrogen Single Cell-to-CT kit (Invitrogen# 4458237) according to the manufacturer's manual. TaqMan assays were used to measure the abundance of *Piezo1*, *Piezo2*, *ChAT*, *Nos1*, *Elavl3*, and *GAPDH*.

Whole-cell patch-clamp recording

Whole-cell patch-clamp recording was done using an Axopatch 200B amplifier (Axon Instruments). Currents were sampled at 20 kHz and filtered at 2 kHz. Mechanical stimulation was applied using a fire-polished glass pipette positioned at an angle of 85° to the cell recorded. The probe was advanced onto the cell by a Clampex controlled piezo-electric crystal microstage (E625 LVPZT Controller/Amplifier; Physik Instrumente). A series of steps in 0.3 μm increments were applied every 10 s, which allowed full recovery from mechanical stimulation. Inward mechanically activated currents were recorded at a holding voltage of -80 mV.

Ex vivo Ca^{2+} imaging

The mouse colon was removed and cut open longitudinally along the mesenteric border. The tissue was pinned flat with the mucosal side up in a chamber coated with Sylgard-184 (Dow Corning Corp., Midland, MI, USA). The sample was bathed in oxygenated (95% oxygen, 5% CO2) Krebs solution. Under a dissecting microscope, the epithelium layer was removed, and the time-lapse movies of calcium imaging were acquired with Leica LAS X software using an inverted Thunder 3D microscope (Leica). Data were processed and analyzed using Leica LAS X software. The brush stimuli were applied by brushing an adjacent area near the field of view using a 0.07 g Von Frey filament (Bioseb). For the shear stress experiment, Krebs solution was delivered at a flow rate of 20 mL/min using a Pump 11 Elite Programmable Syringe Pump (Harvard Apparatus).

CMMC recording

The whole mouse colon (about 5–6 cm) was dissected and placed into oxygenated (95% O2, 5% CO2) Krebs solution. Luminal content was removed through flushing with Krebs solution. The colon preparation was mounted in a horizontal organ bath with oxygenated Krebs solution at 37°C. Preparation was equilibrated for 30 min, and contractile activity was captured using a camera (Logitech, Newark, USA) positioned 10 cm above the colon preparation. After recording, the video was converted to a spatiotemporal map using MATLAB (MathWorks, USA). The frequency of CMMC was analyzed.

Isometric tension recording of colon strips

Colon strips (3 cm in length, full thickness) from the same region were secured at both ends with silk sutures and mounted longitudinally in 25 mL organ baths filled with Krebs solution, aerated with 95% O_2 and 5% CO_2. The tissue was connected to an external force-displacement transducer (World Precision Instruments, Inc.), which was connected to a PowerLab data acquisition system (AD Instruments). Isometric force was recorded, and the frequency of contractions, amplitude, and area under the curve (AUC) were analyzed.

Whole mount microscopy

Colons were flushed with cold HBSS (Thermo Fisher# 14025092), and 1 cm of tissue was placed on a pipette tip. The myenteric plexus was peeled off with a wet Q-tip and pinned down to SYLGARD in 24-well plates. Tissue was then fixed in 2% PFA for 20 minutes, washed with PBS, then blocked and permeabilized for 2 hours in 5% BSA and 0.3% Triton at room temperature. Samples were then incubated overnight with primary antibodies at 4°C in 0.1% Tween20 and 1% BSA antibody solution. The next day, samples were washed 3X in 0.1% Tween20 in PBS (PBSt), then incubated at room temperature for 2 hours with secondary antibodies and directly conjugated primary antibodies in antibody solution. After washing 3X in PBSt, samples were incubated for 10 minutes at room temperature with 1:1,000 DAPI in antibody solution. Samples were washed in PBSt again and mounted on slides with ProLong Gold Antifade mounting media (Invitrogen# 36930). Confocal microscopy was conducted with Zeiss Axio Observer ZI, Leica Upright DM6 and Leica Inverted MDi8 microscopes. Images were processed and analyzed with FIJI. Images were median filtered then background subtracted prior to analysis.

Immunofluorescence

Colons were flushed with cold HBSS, fixed in 4% PFA for 2 hours at 4°C, then dehydrated in 30% sucrose overnight at 4°C. The next day, samples were frozen in Tissue-Tek O.C.T. compound on dry ice and stored in -80°C until 14-16 μm sections were sliced with a Thermo Scientific cryostat. Sections were fixed for 5 minutes at room temperature with 4% PFA and washed PBS. Sections were then permeabilized with 0.1% triton and 2% BSA for 20 minutes and then washed with PBS. Then sections were blocked for 10 minutes with Serum-Free protein Block (Aligent Dako) and washed in PBS again. Sections were incubated overnight at 4°C in primary antibodies in 1% BSA, 0.1% Tween20 antibody solution. The next day, sections were washed with PBSt 3X and stained with secondaries and directly conjugated primary antibodies at room temperature for 1 hour. Samples were washed with PBSt then incubated with 1:1,000 DAPI for 5 minutes. Sections were washed in PBSt, then mounted with ProLong Gold Antifade mounting media (Invitrogen# p36930). Primary antibodies used: c-Fos (1:1000, Cell Signaling Technology# 2250S), HuC/HuD

(1:200, ThermoFisher Scientific #16A11), RFP (1:100, Abcam# ab185921). Directly conjugated primary antibodies and secondaries used: (TUBB3, Biolegend# 801210), Cyanine3 Streptavidin (Biolegend# 405215), Alexa 488 (Invitrogen# A-11008) all 1:1000 dilution and CD11b (Biolegend# 101219) used at 1:200 dilution.

Histology

Colons were dissected but not flushed, and then fixed in Carnoy's fixative (VWR# 101205-852) for two hours on ice. Samples were washed 3x in 70% ethanol. Samples were shipped in 70% ethanol to HistoWiz (HistoWiz.com) for embedding, slicing, and (Alcian Blue/Periodic Acid-Schiff) AB/PAS staining.

Pressure Chamber

Pressure chamber experiments were conducted with a custom-built pressure chamber designed and generously gifted to us by Dr. James Warnock's laboratory.[66] The pressure chamber was acclimated in a 37°C incubator before each use. The pressure chamber was controlled by software from LabVIEW instruments, which was programmed to exert precise oscillating pressure regimes using an air intake valve and an exhaust valve. The air intake valve was connected to a gas tank with 5% CO_2 balanced air consisting of 19.95% O_2 and 80.05% N_2. The intake valve was set to open for 0.6 seconds, and the exhaust was set to open for 0.8 seconds, with a sampling rate of 10 samples per second. For cyclical pressure stimuli, the pressure oscillated between 45 mmHg and 60 mmHg for an amplitude of 15 mmHg. For static pressure stimuli, the exhaust valve was left open and the 45mmHg pressure was used. The regulator on the air tank was slightly manually adjusted throughout the experiments to maintain these pressure levels. For ambient stimuli, cells were placed in the same incubator as the pressure chamber.

Ca^{2+} free c-Fos assay

Colons were flushed with Ca^{2+} free HBSS (ThermoFisher# 14170161) and stimulated with pressure for 5 minutes in Ca^{2+} free HBSS or Ca^{2+} containing HBSS (ThermoFisher# 14025092). 30 minutes later, the myenteric plexus was collected and stained for c-Fos.

Induction of Colitis

Mice were *ad libitum* administered 2.5% dextran sodium sulfate (TdB Labs) in their drinking water for 8 days. On the 8th day, fresh drinking water was administered. Mice were weighed daily at the same time each day. Humane endpoint analysis included weight loss greater than -20%, lethargy, cold to touch, rectal bleeding and/or colon prolapse.

RNA isolation and RT-PCR

Colons were flushed with cold HBSS, and 1 cm colon explants were ruptured with Omni bead rupture tubes in 1 mL TRIzol reagent (Invitrogen), then frozen in -80°C until use. Upon use, 200 μL/1 mL chloroform is added to the tubes. After allowing for phase separation, samples are spun at 4°C for 15 minutes at 12,000 rcf. The middle layer was transferred to RNase free tubes using RNase free pipette tubes. 500 μL isopropanol and 1.5 μL Glycoblue (ThermoFisher Scientific) were added and incubated for 10 minutes before spinning again. The pellet was washed with 75% ethanol and then reconstituted in RNase free water and concentrations were recorded using a NanoDrop. The RNA was converted to cDNA using Maxima H Minus Reverse Transcriptase (Thermofisher # EP0751), RT buffer (Thermofisher# EP0751), Oligo DTs (Thermofisher# SO132), and RNAse OUT (Fisher Sci,# 1077019). Real time qPCR was conducted using AppliedBiosystems QuantStudio5 machine with Universal SYBR Green Supermix (Biorad).

LCN2 ELISA

Fecal samples were collected pre and post induction of DSS-induced colitis and weighed. 0.1% PBS Tween20 was added to samples and vortexed at maximum speed for 10 minutes, then spun down at 12000 RPM at 4 degrees for 10 minutes. Supernatants were collected and used for Mouse LCN2/NGAL Duoset ELISA (R&D Systems# DY1857).

Acetylcholine measurements

Colons were flushed with cold HBSS and 1 cm colon explants were collected, weighed, and added to Assay Buffer VI/Choline Assay Buffer from Choline/Acetylcholine Assay Kit (Abcam# ab65345) in Omni bead rupture tubes (VWR#. 10032-756) and homogenized. Samples were spun down at maximum speed at 4°C for 10 minutes, and supernatants were stored in -80 until measured with colorimetric assay, as per manufacturer's instructions. For measurement of ACh from neurons, supernatant was collected from 450,000 neurons per well and measured with fluorometric assay for increased sensitivity. Choline free media using HBSS (ThermoFisher# 14025092) was used.

Treatment with Piezo1 pharmacological modulators

Differentiated neurons or 1 cm colon explants were treated for 5 minutes with 5 μM Yoda1 (Sigma# SML1558) in media consisting of DMEM (ThermoFisher# 10313021), 1 mL B27 (ThermoFisher# 17504044), 500 μL FBS-C, 500 μL L-glutamine (ThermoFIsher # 25030081), 50 μL Glial Derived Neurotrophic factor (ThermoFisher# 4504410UG), and 500 μL antibiotic/antimycotic

(ThermoFisher# 15240062). After 5 minutes, the media was washed out and staining was conducted 30 minutes later. For Piezo1 antagonism, neurons were treated with 10 μM GsMTx-4 (Abcam# ab141871) for 5 minutes.

Isolation of cells from the colon

Isolation of cells from the colon was performed as previously described.[8] Specifically, the colon was harvested and washed with Hanks balanced salt solution (HBSS) before being longitudinally cut open. The colon pieces were transferred to a conical tube containing 12 ml HBSS supplemented with 5 mM EDTA and 1 mM Dithiothreitol (DTT) and put on a shaker at 37°C for 20 minutes. The epithelial sheet was removed by vigorous manual shaking of the tube for 15 seconds. Subsequently, the tissue was transferred to fresh HBSS containing DTT and EDTA and shaken at 37°C for an additional 20 minutes, after which any remaining epithelial cells were removed by further vigorous manual shaking for 15 seconds. The tissue was then washed by vigorous shaking for 15 seconds in HBSS. Next, the colon pieces were taken out and finely minced with small scissors. The cut pieces were resuspended in 3 ml of RPMI with 5% FBS in a 50 ml conical tube. An additional 3 ml 2x digestion buffer was added to achieve final concentrations of 1 mg/ml collagenase D and 50 μg/ml DNase in RPMI with 5% FBS. The mixture was then incubated at 37° with shaking for 30 minutes. Following digestion, the reaction was quenched with RPMI with 5% FBS and put through a metal strainer. The back of a 5 ml syringe was used to mash through a metal strainer, followed by thorough washing. The resulting mixture was further filtered through a 70 μm cell strainer with thorough washing of the strainer. Finally, the mixture was centrifuged and ready for flow cytometry.

Flow cytometry

Staining of cells was performed as previously described.[67] Antibodies used from Biolegend include Ly6C-FITC (clone HK1.4), MHCII-PE (clone M5/114.15.2), CD64-APC (clone x54-5/7.1), SiglecF-PE-cy7 (clone S17007L), EpCam-APC-cy7 (clone G8.8), Ly6G-BV421 (clone 1A8), CD11c-BV605 (clone N418), CD11b-BV711 (clone M1/70), CD45-FITC (clone 30-F11), NK.1-PE (clone PK136), CD8-APC (clone 53-6.7), B220-BV421 (clone RA3-6B2), TCRβ-BV605 (clone H57-597), CD4-BV711 (clone RM4-5), CD11b-PE-y7 (clone M1/70), CD16/32 (clone 93). From BD biosciences we used CD45-BV395 (clone 30-F11) and Live/Dead BV510 (BD#564406). Flow cytometry data were acquired on a BD FACSymphony A5 Cell Analyzer with FACSDiva software and were analyzed with FlowJo software (TreeStar).

QUANTIFICATION AND STATISTICAL ANALYSIS

Data analysis was conducted using GraphPad Prism (version 10.3.1). Unless otherwise stated, data are presented with mean bars and/or expressed as mean ± SE. For data disturbed normally, unpaired student t-tests (two-tailed) were used to compare 2 groups while one-way ANOVA or two-way ANOVA with Bonferroni test were used to compare three or more groups. Where applicable data was presented as the S.E.M.A p value lower than 0.05 was considered significant. * ($p < 0.05$), ** ($p < 0.01$), *** ($p < 0.001$), or **** ($p < 0.0001$). Schematics were made using BioRender software.

CellPress

Supplemental figures

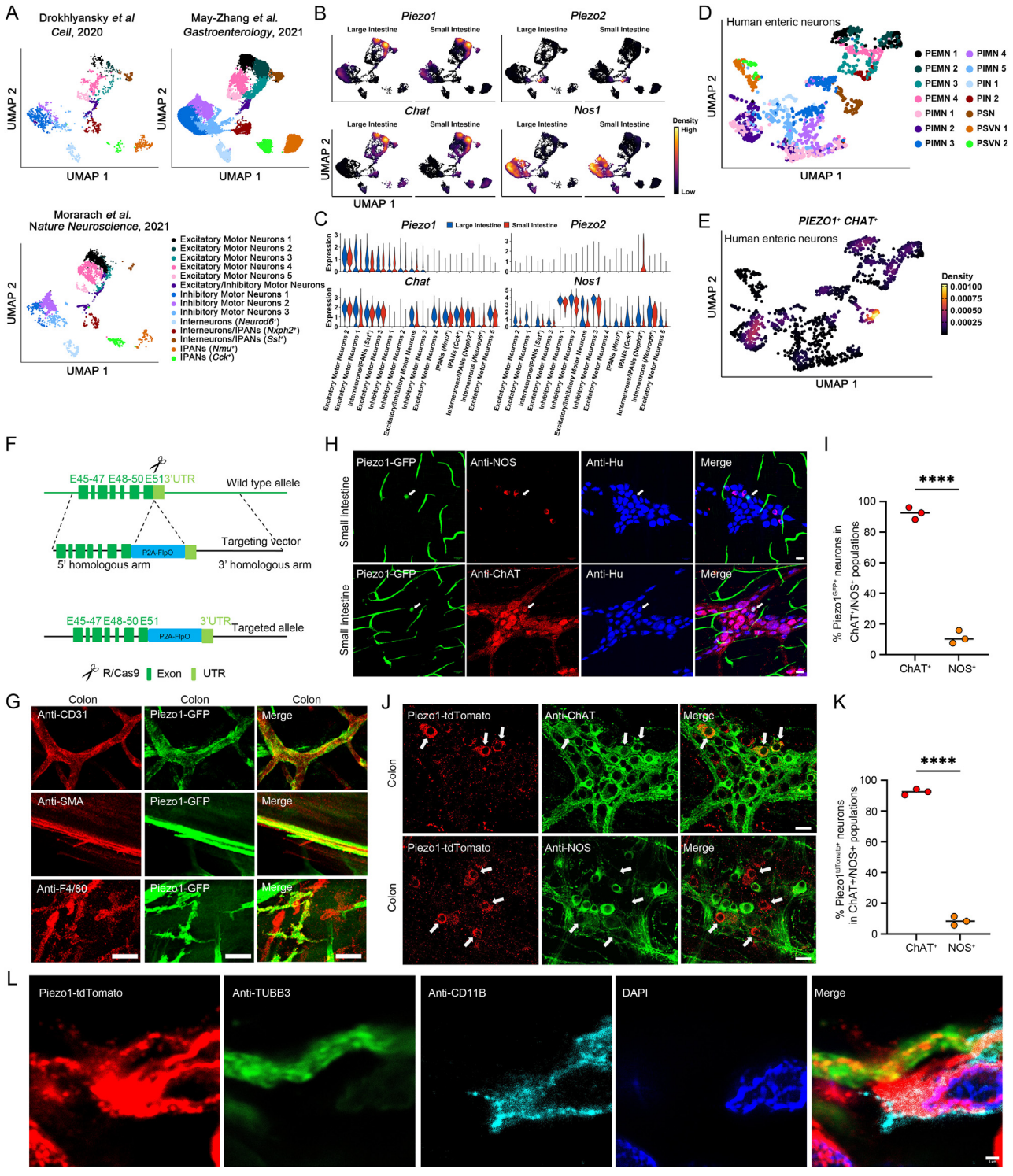

(legend on next page)

Figure S1. Piezo1 is expressed in cholinergic enteric neurons, related to Figure 1

(A) UMAP analysis of scRNA-seq from 3 ENS datasets,[25–27] after batch correction using harmony.

(B) UMAP showing expression of *Piezo1*, *Piezo2*, *Chat*, and *Nos1* in the small versus large intestine from mined datasets of Drokhlyansky et al.,[25,26] Morarach et al.,[25,26] and May-Zhang et al.[27]

(C) Density and violin plots showing expression of *Piezo1*, *Piezo2*, *Chat*, and *Nos1* in the small versus large intestine in the 14 distinct ENS clusters from mined datasets of Drokhlyansky et al.,[25,26] Morarach et al.,[25,26] and May-Zhang et al.[27]

(D) UMAP of human ENS distinct populations mined from scRNA-seq from Drokhlyansky et al.[25]

(E) UMAP showing the co-expression of *CHAT*$^+$ and *PIEZO1*$^+$ human enteric neurons mined from scRNA-seq from Drokhlyansky et al.[25]

(F) Schematic diagram of the generation of Piezo1-flpo transgenic mice.

(G) Representative immunofluorescence images of Piezo1-GFP$^+$ endothelial cells (red, top), smooth muscle cells (red, middle), and macrophages (red, bottom) co-stained with anti-GFP (middle vertical) from whole-mount colon myenteric plexus preparations from Piezo1^{flpo}-GFP reporter mice. Scale bar: 25 μm.

(H) Representative immunofluorescence images of Piezo1-GFP$^+$ neurons (green) stained for anti-GFP (green), anti-NOS (top, red), or anti-ChAT (bottom, red) and anti-Hu (blue) from whole-mount small intestine myenteric plexus preparations from Piezo1^{flpo}-GFP reporter mice. Scale bar: 25 μm.

(I) Summary data showing the percentage of Piezo1-GFP$^+$ myenteric neurons among the ChAT$^+$, and NOS$^+$ ENS populations. ****$p < 0.0001$, two-tailed Student's t test.

(J) Representative immunofluorescence images of Piezo1-tdTomato$^+$ myenteric plexus neurons in whole-mount colon preparations from the Piezo1^{tdTomato} reporter mice, co-stained with anti-RFP (red, left), anti-ChAT (green, top middle), or anti-NOS (green, bottom, middle) and merged images (right). Scale bar: 25 μm.

(K) Summary data showing the percentage of Piezo1-tdTomato$^+$ enteric neurons among the ChAT$^+$, and NOS$^+$ ENS populations. ****$p < 0.0001$, two-tailed Student's t test.

(L) Representative immunofluorescence images of Piezo1-tdTomato$^+$ enteric neurons in the mucosa, co-stained with anti-RFP (red), anti-TUBB3 (green), CD11b (cyan), and merged with DAPI (gray, right), in colonic enteric neurons of Piezo1^{tdTomato} reporter mice. Scale bar: 1 μm.

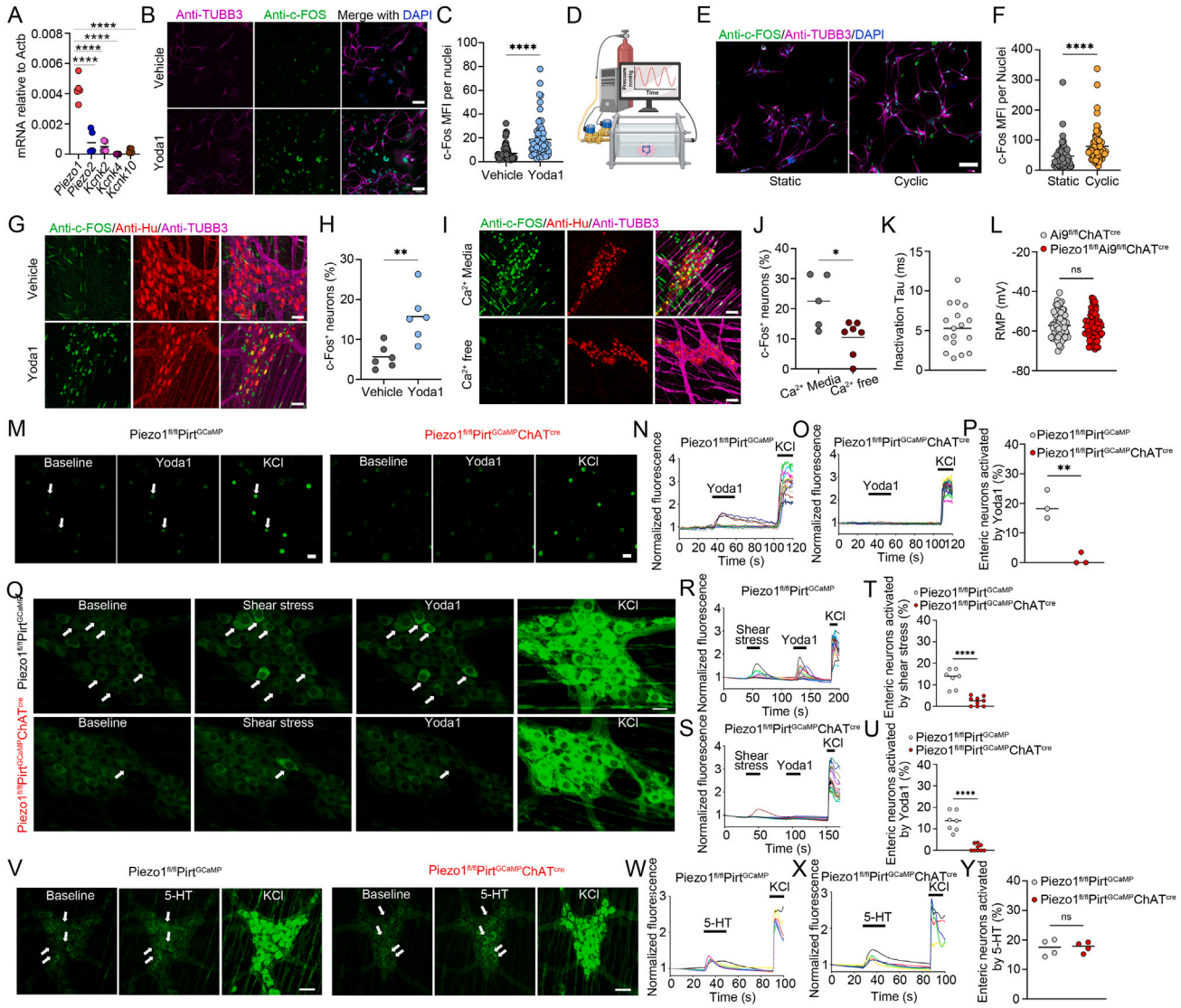

Figure S2. Piezo1 in cholinergic enteric neurons responds to mechanical force, related to Figure 2

(A) Gene expression of mechanosensory ion channels relative to β-actin from differentiated enteric neurons isolated from the myenteric plexus of WT mice analyzed by real-time RT-qPCR. Data representative of 3 biological replicates. ****$p < 0.0001$, two-tailed Student's t test.

(B) Representative image of differentiated enteric neuron culture stained with anti-beta tubulin (magenta), Anti-c-Fos (green), and DAPI (blue) 30 min after a 5-min stimulation with DMSO (top) or Yoda1 (bottom). Scale bar: 78 μm.

(C) Summary data of the mean fluorescence intesity (MFI) of each neuronal nucleus normalized to the area of the nucleus as in (B). ****$p < 0.0001$, two-tailed Student's t test.

(D) Schematic of cyclical hydrostatic pressure bioreactor showing side view.

(E) Representative image of differentiated enteric neuron culture stained with anti-beta tubulin (magenta), anti-c-Fos (green), and DAPI (blue) 30 min after a 5-min stimulation with static (left) or cyclic (right) pressure. Scale bar: 78 μm.

(F) Summary data of the MFI of each neuronal nucleus normalized to the area of the nucleus as in (E). ****$p < 0.0001$, two-tailed Student's t test.

(G) Representative confocal immunofluorescence image of isolated colonic myenteric plexus stained for anti-HuC/HuD (red), anti-c-Fos (green), and anti-beta tubulin (magenta) from vehicle-treated (top) and Yoda1-treated (bottom) colon explants. Scale bar: 78 μm.

(H) Quantification of the ratio of c-Fos$^+$ neuron cell bodies to total neuron cell bodies stained in (G). **$p < 0.01$, two-tailed Student's t test.

(I) Representative confocal immunofluorescence image of anti-Hu (red), anti-c-Fos (green), and anti-beta tubulin (magenta) in pressure-treated colon explants in Ca^{2+}-positive (top) or Ca^{2+}-free media (bottom). Scale bar: 78 μm.

(J) Quantification of the ratio of c-Fos$^+$ neuron cell bodies to total neuron cell bodies stained in (I). *$p < 0.05$, two-tailed Student's t test.

(K) Inactivation time constants of mechanically activated whole-cell currents in isolated enteric neurons.

(L) Resting membrane potential was measured in tdTomato$^+$ enteric neurons from Ai9$^{fl/fl}$ChAT^{cre} and Piezo1$^{fl/fl}$Ai9$^{fl/fl}$ChAT^{cre}, and no significant differences were observed. $n = 67$ cells from 5 mice for Ai9$^{fl/fl}$ChAT^{cre}, and $n = 62$ cells from 5 mice for Piezo1$^{fl/fl}$Ai9$^{fl/fl}$ChAT^{cre} mice. ns, no significant difference, two-tailed Student's t test.

(legend continued on next page)

(M) Representative single frames taken from GCaMP3 fluorescence recordings of colonic myenteric neurons isolated from Piezo1$^{fl/fl}$Pirt^{GCaMP} (left) and Piezo1$^{fl/fl}$Pirt^{GCaMP}ChAT^{cre} (right) mice before and after 10 μM Yoda1 and 100 mM KCl stimuli. Responsive neurons are marked with white arrows. Scale bar: 20 μm.

(N) Representative time-lapse traces of 10 μM Yoda1-induced GCaMP3 signals in colonic myenteric neurons isolated from Piezo1$^{fl/fl}$Pirt^{GCaMP} mice.

(O) Representative time-lapse traces of 10 μM Yoda1-induced GCaMP3 signals in colonic myenteric neurons isolated from Piezo1$^{fl/fl}$Pirt^{GCaMP}ChAT^{cre} mice.

(P) Quantification of colonic myenteric neurons activated by 10 μM Yoda1. $n = 3$ from both Piezo1$^{fl/fl}$Pirt^{GCaMP} and Piezo1$^{fl/fl}$Pirt^{GCaMP}ChAT^{cre} mice. $^{**}p < 0.01$, two-tailed Student's t test.

(Q) Representative single frames taken from GCaMP3 fluorescence recordings of neurons within whole-mount colonic myenteric plexus from Piezo1$^{fl/fl}$Pirt^{GCaMP} (top) and Piezo1$^{fl/fl}$Pirt^{GCaMP}ChAT^{cre} (bottom) mice subjected to sheer stress (20 mL/min flow stimulus), 10 μM Yoda1, and 100 mM KCl applications. Responsive neurons are marked with white arrows. Scale bar: 25 μm.

(R) Representative time-lapse traces of GCaMP3 signals induced by sheer stress and 10 μM Yoda1 in whole-mount myenteric plexus neurons from Piezo1$^{fl/fl}$Pirt^{GCaMP} mice. 100 mM KCl was used as the positive control.

(S) Representative time-lapse traces of GCaMP3 signals induced by sheer stress and 10 μM Yoda1 in whole-mount myenteric plexus neurons from and Piezo1$^{fl/fl}$Pirt^{GCaMP}ChAT^{cre} mice. 100 mM KCl was used as the positive control.

(T) The proportions of colonic myenteric neurons activated by sheer stress in Piezo1$^{fl/fl}$Pirt^{GCaMP} and Piezo1$^{fl/fl}$Pirt^{GCaMP}ChAT^{cre} mice. $^{****}p < 0.0001$, two-tailed Student's t test.

(U) The proportions of colonic myenteric neurons activated by 10 μM Yoda1 in Piezo1$^{fl/fl}$Pirt^{GCaMP} and Piezo1$^{fl/fl}$Pirt^{GCaMP}ChAT^{cre} mice. $^{****}p < 0.0001$, two-tailed Student's t test.

(V) Representative single frames are taken from GCaMP3 fluorescence recordings of neurons within whole-mount colonic myenteric plexus from Piezo1$^{fl/fl}$Pirt^{GCaMP} and Piezo1$^{fl/fl}$Pirt^{GCaMP}ChAT^{cre} mice before and after 10 μM 5-HT and 100 mM KCl applications. Responsive neurons are marked with white arrows. Scale bar: 50 μm.

(W) Representative time-lapse traces of 10 μM 5-HT-induced GCaMP3 signals in colonic myenteric plexus neurons from Piezo1$^{fl/fl}$Pirt^{GCaMP} mice. 100 mM KCl was used as positive control.

(X) Representative time-lapse traces of 10 μM 5-HT-induced GCaMP3 signals in colonic myenteric plexus neurons from Piezo1$^{fl/fl}$Pirt^{GCaMP}ChAT^{cre} mice. 100 mM KCl was used as positive control.

(Y) The proportions of enteric neurons from Piezo1$^{fl/fl}$Pirt^{GCaMP} and Piezo1$^{fl/fl}$Pirt^{GCaMP}ChAT^{cre} mice activated by 10 μM 5-HT. $n = 4$ for both Piezo1$^{fl/fl}$Pirt^{GCaMP} and Piezo1$^{fl/fl}$Pirt^{GCaMP}ChAT^{cre} mice. ns, no significant difference, two-tailed Student's t test.

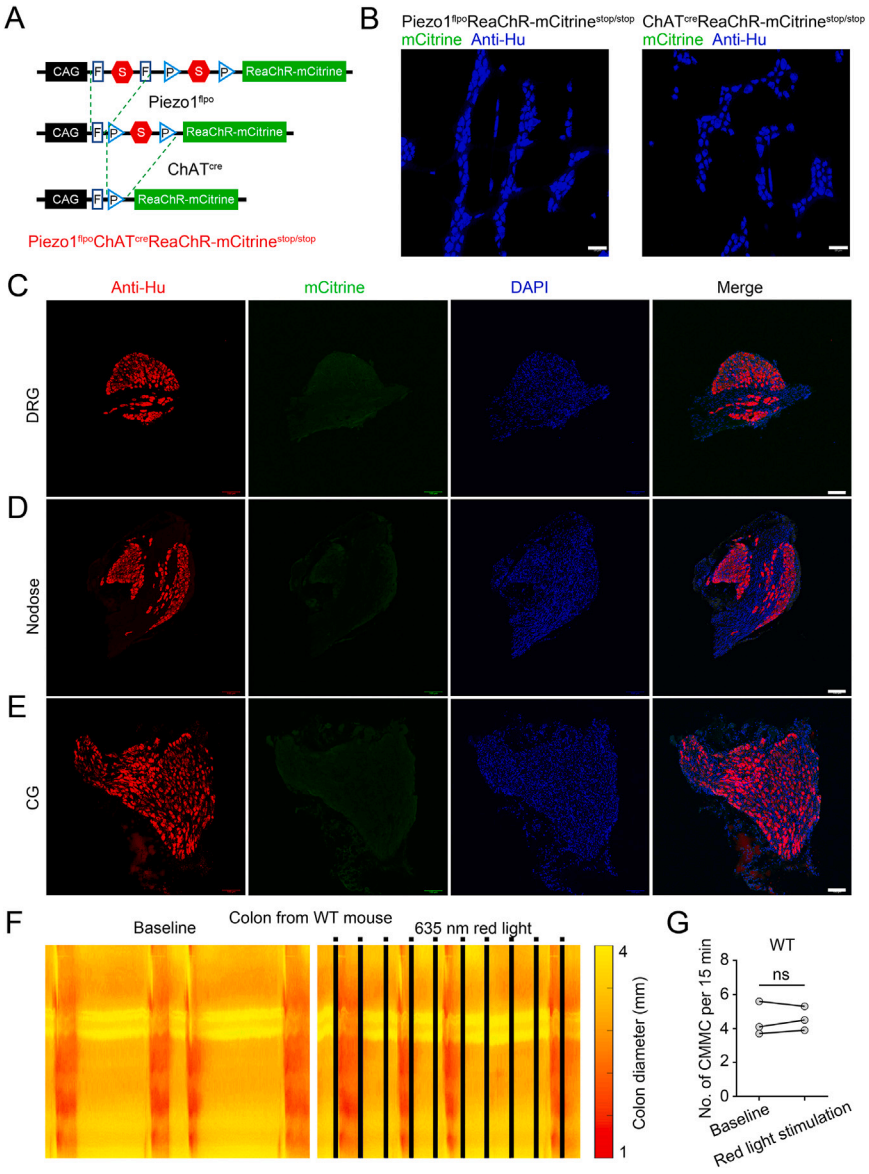

Figure S3. Intersectional strategy to optogenetically activate cholinergic Piezo1^{+} enteric neurons, related to Figure 3

(A) Schematic of genetic approach to generate Piezo1^{flpo}ChAT^{cre}ReaChR-mCitrine$^{stop/stop}$ mice.

(B) Representative confocal images of whole-mount myenteric plexus preparations from Piezo1^{flpo}ReaChR-mCitrine$^{stop/stop}$ (left) and ChAT^{cre}ReaChR-mCitrine$^{stop/stop}$ (right) mice showing no mCitrine without double positive. Scale bar: 50 μm.

(C) Representative confocal images of Piezo1^{flpo}ChAT^{cre}ReaChR-mCitrine$^{stop/stop}$ in DRG. Scale bar: 100 μm.

(D) Representative confocal images of Piezo1^{flpo}ChAT^{cre}ReaChR-mCitrine$^{stop/stop}$ in nodose ganglia. Scale bar: 100 μm.

(E) Representative confocal images of Piezo1^{flpo}ChAT^{cre}ReaChR-mCitrine$^{stop/stop}$ in celiac ganglia (CG). Scale bar: 100 μm.

(F) Representative spatiotemporal maps of CMMC recordings for a colon prep isolated from WT mice, with (right) and without (left) red light stimulation.

(G) Quantification of CMMC frequencies within a 15-min time frame under both baseline and red light stimulation in WT mice. ns, no significant difference, paired Student's t test.

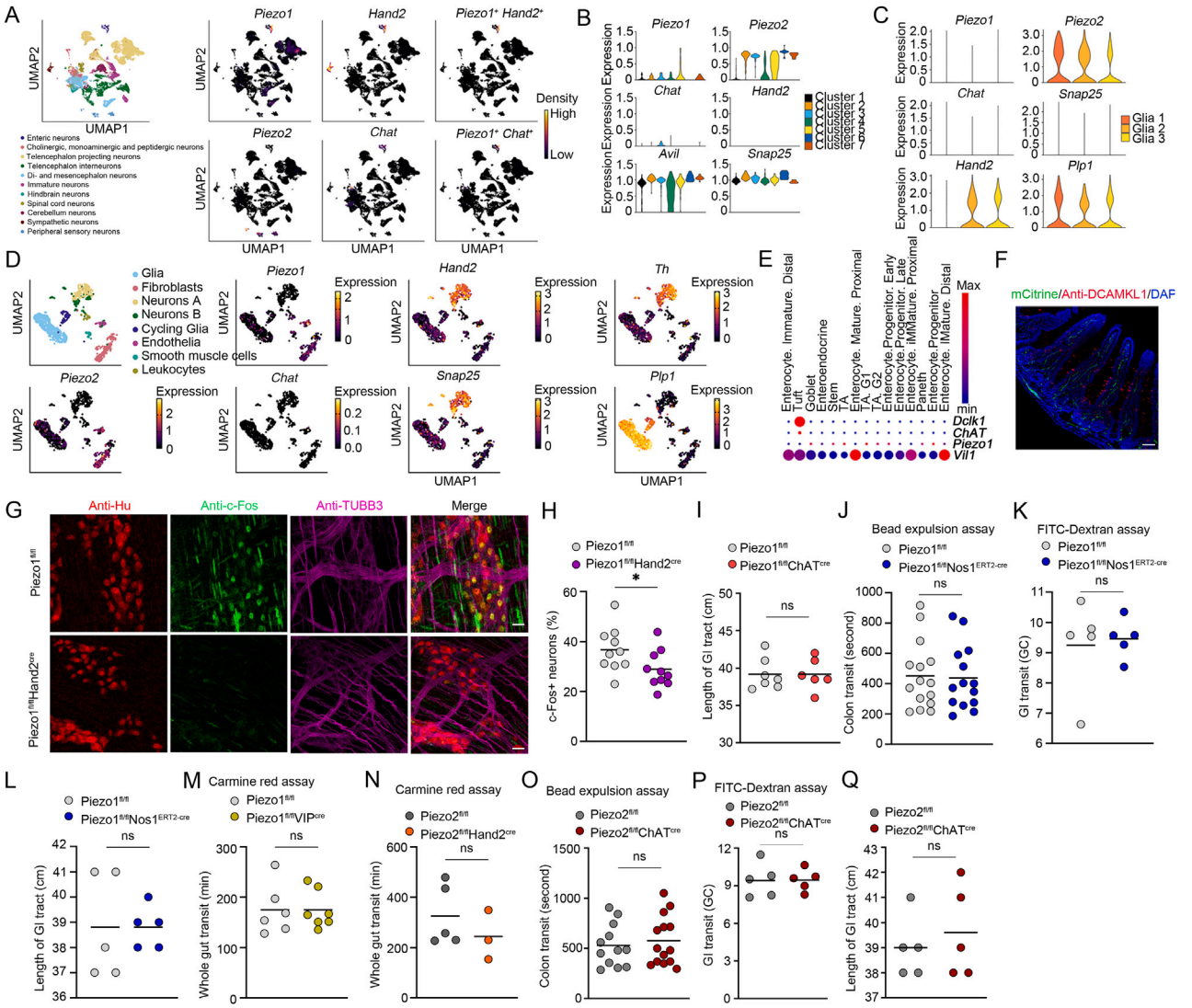

Figure S4. Piezo1 is specifically expressed and functional in intrinsic cholinergic enteric neurons, related to Figure 5

(A) UMAP of scRNA-seq datasets from Zeisel et al.[37] of all mouse neuronal populations and UMAPs showing *Piezo1*-, *Piezo2*-, *Hand2*-, and *Chat*-positive neuronal populations. Note that *Piezo1* and *Hand2* co-expression as well as *Piezo1* and *Chat* co-expression only occurs in enteric neuronal populations.

(B) Density and violin plots of *Piezo1*, *Piezo2*, *Chat*, *Hand2*, *Avil*, and *Snap25* in 7 subsets of extrinsic sensory neurons that innervate the colon mined from Hockley et al.[38]

(C) Density and violin plots depicting expression of *Piezo1*, *Piezo2*, *Chat*, *Snap25*, *Hand2*, and *Plp1* in 3 subsets of enteric glia mined from RNA-seq datasets from Drokhlyansky et al.[25]

(D) UMAP plots depicting expression of *Piezo1*, *Piezo2*, *Chat*, *Hand2*, *Snap25*, *Th*, and *Plp1* in sympathetic neurons from the CG mined from RNA-seq datasets from Sivori et al.[62]

(E) Dot plot depicting gene expression from scRNA-seq of intestinal epithelium mined from Haber et al.[41]

(F) Representative confocal images of the small intestine sections from Piezo1^{flpo}ChAT^{cre}ReaChR-mCitrine$^{stop/stop}$ mice stained for anti-GFP (green) and anti-DCAMKL1 (red) showing no tuft cell overlap with Piezo1. Scale bar: 50 μm.

(G) Representative confocal immunofluorescence images of isolated colonic myenteric plexus stained for anti-Hu (red), anti-c-Fos (green), and anti-beta tubulin (magenta) from Piezo1$^{fl/fl}$ (top) and Piezo1$^{fl/fl}$Hand2^{cre} (bottom) mice. Scale bar: 78 μm.

(H) Quantification of the ratio of c-Fos^{+} neuron cell bodies to total neuron cell bodies stained in (A). *$p < 0.05$, two-tailed Student's t test.

(I) Summary data of GI tract length in Piezo1$^{fl/fl}$ and Piezo1$^{fl/fl}$ChAT^{cre} cohoused mice. ns, no significant difference, two-tailed Student's t test.

(J) Quantification of *in vivo* colon transit time via bead expulsion assay in Piezo1$^{fl/fl}$ and Piezo1$^{fl/fl}$Nos1$^{ERT2\text{-}cre}$ mice. ns, no significant difference, two-tailed Student's t test.

(K) Summary data showing *in vivo* GI transit via FITC-dextran assay in Piezo1$^{fl/fl}$ and Piezo1$^{fl/fl}$Nos1$^{ERT2\text{-}cre}$ mice. ns, no significant difference, two-tailed Student's t test.

(L) Summary data of GI tract length in Piezo1$^{fl/fl}$ and Piezo1$^{fl/fl}$Nos1$^{ERT2\text{-}cre}$ mice. ns, no significant difference, two-tailed Student's t test.

(M) Summary data showing *in vivo* GI transit via carmine red assay in Piezo1$^{fl/fl}$ and Piezo1$^{fl/fl}$VIP^{cre} mice. ns, no significant difference, two-tailed Student's t test.

(legend continued on next page)

(N) Summary data showing *in vivo* GI transit via carmine red assay in Piezo2$^{fl/fl}$ and Piezo2$^{fl/fl}$Hand2^{cre} mice. ns, no significant difference, two-tailed Student's t test.
(O) Quantification of *in vivo* colon transit time via bead expulsion assay in Piezo2$^{fl/fl}$ and Piezo2$^{fl/fl}$ChAT^{cre} mice. ns, no significant difference, two-tailed Student's t test.
(P) Summary data showing *in vivo* GI transit via FITC-dextran assay in Piezo2$^{fl/fl}$ and Piezo2$^{fl/fl}$ChAT^{cre} mice. ns, no significant difference, two-tailed Student's t test.
(Q) Summary data of GI tract length in Piezo2$^{fl/fl}$ and Piezo2$^{fl/fl}$ChAT^{cre} mice. ns, no significant difference, two-tailed Student's t test.

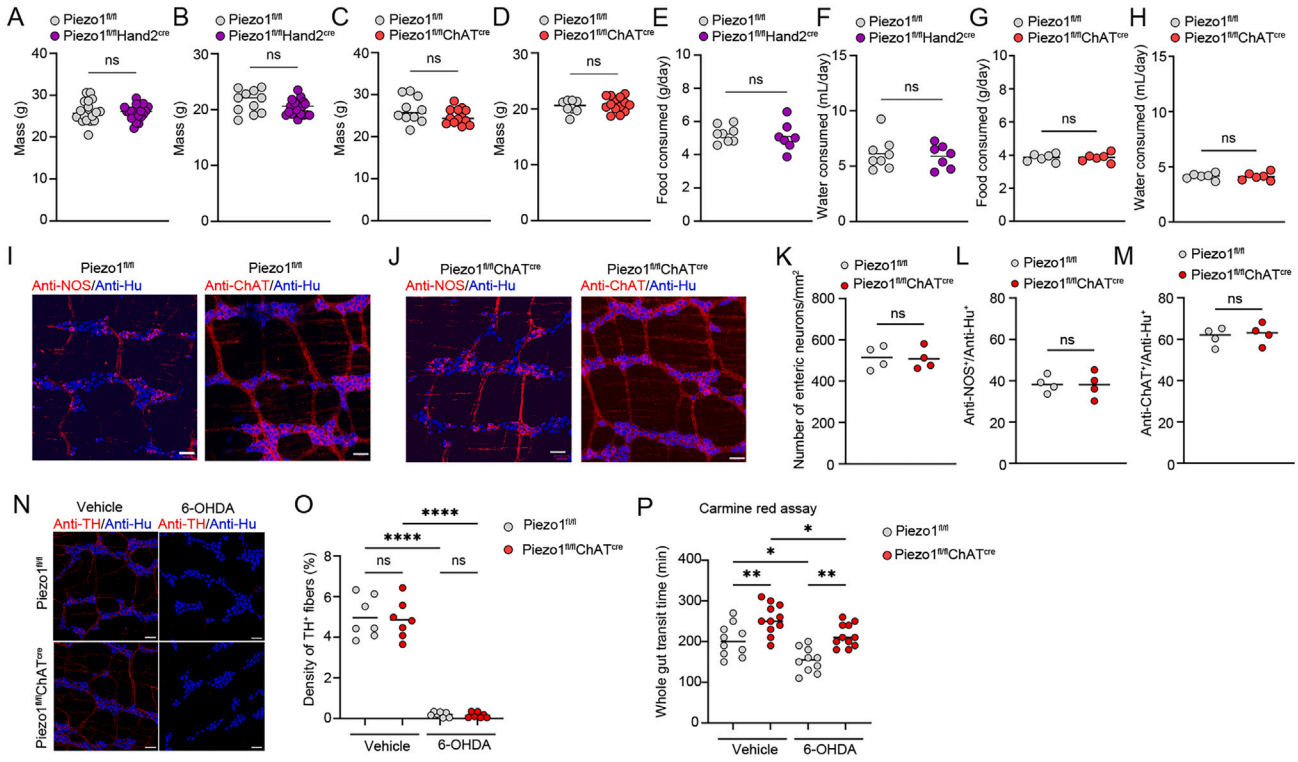

Figure S5. Enteric cholinergic neuronal Piezo1 does not affect ENS development and operates independently of sympathetic innervation, related to Figure 5

(A) Summary data of baseline mass of male Piezo1$^{fl/fl}$ and Piezo1$^{fl/fl}$Hand2^{cre} mice. ns, no significant difference, two-tailed Student's t test.

(B) Summary data of baseline mass of female Piezo1$^{fl/fl}$ and Piezo1$^{fl/fl}$Hand2^{cre} mice. ns, no significant difference, two-tailed Student's t test.

(C) Summary data of baseline mass of male Piezo1$^{fl/fl}$ and Piezo1$^{fl/fl}$ChAT^{cre} mice. ns, no significant difference, two-tailed Student's t test.

(D) Summary data of baseline mass of female Piezo1$^{fl/fl}$ and Piezo1$^{fl/fl}$ChAT^{cre} mice. ns, no significant difference, two-tailed Student's t test.

(E) Summary data of average quantity of food consumed per day per mouse in Piezo1$^{fl/fl}$ and Piezo1$^{fl/fl}$Hand2^{cre} mice. Each data point represents 2–5 mice. ns, no significant difference, two-tailed Student's t test.

(F) Summary data of average quantity of water consumed per day per mouse in Piezo1$^{fl/fl}$ and Piezo1$^{fl/fl}$Hand2^{cre} mice. Each data point represents 2–5 mice. ns, no significant difference, two-tailed Student's t test.

(G) Summary data of average quantity of food consumed per day per mouse in Piezo1$^{fl/fl}$ and Piezo1$^{fl/fl}$ChAT^{cre} mice. Each data point represents 2–5 mice. ns, no significant difference, two-tailed Student's t test.

(H) Summary data of average quantity of water consumed per day per mouse in Piezo1$^{fl/fl}$ and Piezo1$^{fl/fl}$ChAT^{cre} mice. Each data point represents 2–5 mice. ns, no significant difference, two-tailed Student's t test.

(I) Representative confocal images of whole-mount myenteric plexus preparations from Piezo1$^{fl/fl}$ mice stained for anti-NOS (left), anti-ChAT (right), and anti-Hu (blue). Scale bar: 50 μm.

(J) Representative confocal images of whole-mount myenteric plexus preparations from Piezo1$^{fl/fl}$ChAT^{cre} mice stained for anti-NOS (left), anti-ChAT (right), and anti-Hu (blue). Scale bar: 50 μm.

(K) Summary data of number of enteric neurons per mm^2 between whole-mount myenteric plexus preparations from Piezo1$^{fl/fl}$ and Piezo1$^{fl/fl}$ChAT^{cre} mices. ns, no significant difference, two-tailed Student's t test.

(L) Summary data of the ratio of anti-NOS$^+$ to anti-Hu$^+$ neurons in whole-mount myenteric plexus preparations from Piezo1$^{fl/fl}$ and Piezo1$^{fl/fl}$ChAT^{cre} mice. ns, no significant difference, two-tailed Student's t test.

(M) Summary data of the ratio of anti-ChAT$^+$ to anti-Hu$^+$ neurons in whole-mount myenteric plexus preparations from Piezo1$^{fl/fl}$ and Piezo1$^{fl/fl}$ChAT^{cre} mice. ns, no significant difference, two-tailed Student's t test.

(N) Representative confocal images of anti-TH (red) and anit-Hu (blue) staining in the myenteric plexus of Piezo1$^{fl/fl}$ (top) and Piezo1$^{fl/fl}$ChAT^{cre} (bottom) mice treated with vehicle (left) or 6-OHDA (right). Scale bar: 50 μm.

(O) Summary data of the density of TH$^+$ fibers in Piezo1$^{fl/fl}$ and Piezo1$^{fl/fl}$ChAT^{cre} mice treated with vehicle or 6-OHDA. ns, not significant, ****$p < 0.0001$, one-way ANOVA.

(P) Summary data showing *in vivo* GI transit via carmine red assay in Piezo1$^{fl/fl}$ and Piezo1$^{fl/fl}$ChAT^{cre} mice treated with vehicle or 6-OHDA. *$p < 0.05$, **$p < 0.01$, one-way ANOVA.

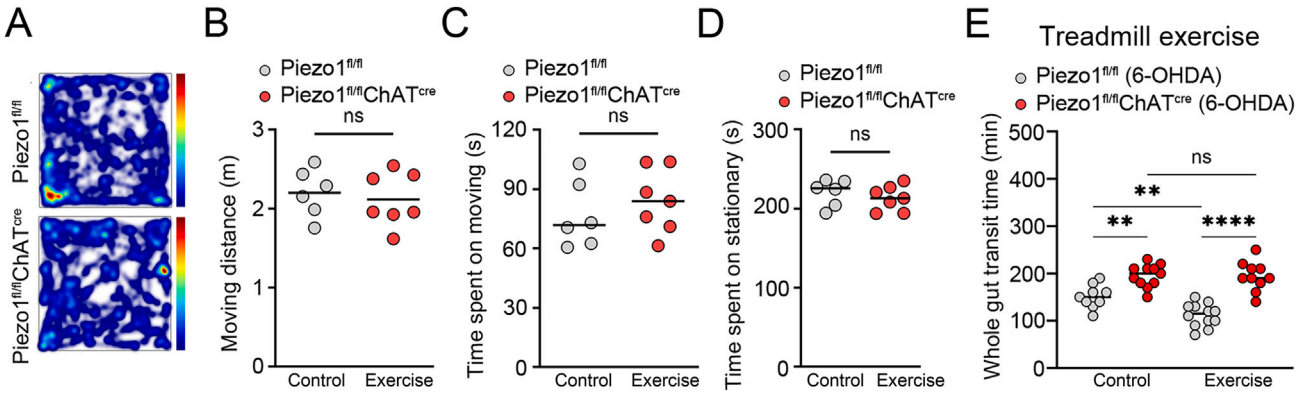

Figure S6. Cholinergic Piezo1 does not regulate voluntary movement or sympathetic neuronal activity during exercise induced motility, related to Figure 6

(A) Representative images illustrate heatmaps of voluntary movements of Piezo1$^{fl/fl}$ and Piezo1$^{fl/fl}$ChAT^{cre} mice.

(B–D) Summary data showing total moving distance (B), total time spent moving (C), total time spent stationary (D) of voluntary movement of Piezo1$^{fl/fl}$ and Piezo1$^{fl/fl}$ChAT^{cre} mice. ns, no significant difference, two-tailed Student's t test.

(E) Summary data showing the impact of 10-min treadmill exercise on GI transit via carmine red assay in Piezo1$^{fl/fl}$ and Piezo1$^{fl/fl}$ChAT^{cre} mice treated with 6-OHDA. ns, no significant difference, $^{**}p < 0.01$, $^{****}p < 0.0001$, one-way ANOVA.

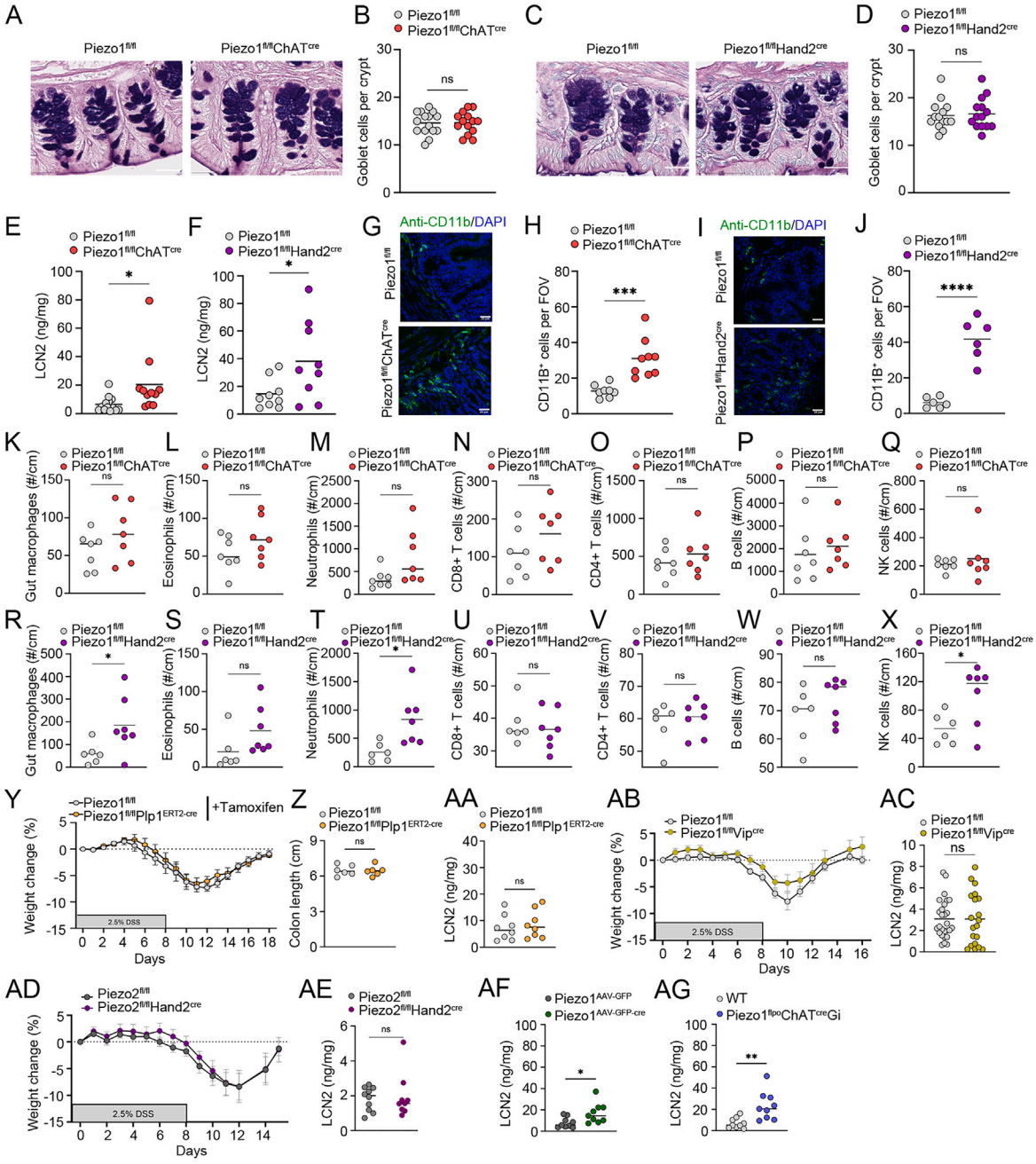

Figure S7. Piezo1 in enteric cholinergic neurons ameliorates colitis severity, related to Figure 7

(A) Representative AB/PAS staining of colon sections obtained from cohoused Piezo1$^{fl/fl}$ and Piezo1$^{fl/fl}$ChAT^{cre} littermates at steady state. Scale bar: 50 μm.

(B) Enumeration of goblet cells per crypt in AB/PAS histological sections from cohoused Piezo1$^{fl/fl}$ and Piezo1$^{fl/fl}$ChAT^{cre} mice at steady state. ns, no significant difference, two-tailed Student's t test.

(C) Representative AB/PAS staining of colon sections obtained from cohoused Piezo1$^{fl/fl}$ and Piezo1$^{fl/fl}$Hand2^{cre} mice at steady state. Scale bar: 50 μm.

(D) Enumeration of goblet cells per crypt in AB/PAS histological sections from cohoused Piezo1$^{fl/fl}$ and Piezo1$^{fl/fl}$Hand2^{cre} mice at steady state. ns, no significant difference, two-tailed Student's t test.

(E) Summary data of fecal LCN2 production measured via ELISA from Piezo1$^{fl/fl}$ and Piezo1$^{fl/fl}$ChAT^{cre} cohoused mice post DSS administration. *$p < 0.05$, two-tailed Student's t test.

(F) Summary data of fecal LCN2 production measured via ELISA from Piezo1$^{fl/fl}$ and Piezo1$^{fl/fl}$Hand2^{cre} cohoused mice 28 days post DSS administration. *$p < 0.05$, two-tailed Student's t test.

(G) Representative confocal images of day 8 DSS colons taken from Piezo1$^{fl/fl}$ and Piezo1$^{fl/fl}$ChAT^{cre} mice, stained for CD11b (green) and merged with DAPI (blue). Scale bar: 20 μm.

(legend continued on next page)

(H) Enumeration of CD11b^{+} cells per field of view in Piezo1$^{fl/fl}$ and Piezo1$^{fl/fl}$ChAT^{cre} mice. ***$p < 0.001$, two-tailed Student's t test.
(I) Representative confocal images of day 8 DSS colons taken from Piezo1$^{fl/fl}$ and Piezo1$^{fl/fl}$Hand2^{cre} mice, stained for CD11b (green) and merged with DAPI (blue). Scale bar: 20 μm.
(J) Enumeration of CD11b^{+} cells per field of view in Piezo1$^{fl/fl}$ and Piezo1$^{fl/fl}$Hand2^{cre} mice. ****$p < 0.0001$, two-tailed Student's t test.
(K–Q) Summary data of the number of gut macrophages (K), eosinophils (L), neutrophils (M), CD8^{+} T cells (N), CD4^{+} T cells (O), B cells (P), and NK cells (Q), recruited per colon length in Piezo1$^{fl/fl}$ and Piezo1$^{fl/fl}$ChAT^{cre} mice post 8-day administration of DSS. ns, no significant difference, two-tailed Student's t test.
(R–X) Summary data of the number of gut macrophages (R), eosinophils (S), neutrophils (T), CD8^{+} T cells (U), CD4^{+} T cells (V), B cells (W), and NK cells (X), recruited per colon length in Piezo1$^{fl/fl}$ and Piezo1$^{fl/fl}$Hand2^{cre} mice post 8-day administration of DSS. *$p < 0.05$, ns, no significant difference, two-tailed Student's t test.
(Y) Weight loss of cohoused Piezo1$^{fl/fl}$ ($n = 11$) and Piezo1$^{fl/fl}$Plp1$^{ERT2\text{-}cre}$ ($n = 11$) mice. Mice were administered 2.5% DSS in their drinking water for 7 days. Data are expressed as mean ± SE.
(Z) Summary data of colon length shortening post DSS administration in Piezo1$^{fl/fl}$ and Piezo1$^{fl/fl}$Plp1$^{ERT2\text{-}cre}$ cohoused mice. ns, no significant difference; two-tailed Student's t test.
(AA) Summary data of fecal LCN2 production measured via ELISA from Piezo1$^{fl/fl}$ and Piezo1$^{fl/fl}$Plp1$^{ERT2\text{-}cre}$ cohoused mice post DSS administration. ns, no significant difference, two-tailed Student's t test.
(AB) Weight loss of cohoused Piezo1$^{fl/fl}$ ($n = 23$) and Piezo1$^{fl/fl}$VIP^{cre} ($n = 16$) mice. Mice were administered 2.5% DSS in their drinking water for 8 days. Data are expressed as mean ± SE.
(AC) Summary data of fecal LCN2 production measured via ELISA from Piezo1$^{fl/fl}$ and Piezo1$^{fl/fl}$VIP^{cre} cohoused mice 28 days post DSS administration. ns, two-tailed Student's t test.
(AD) Weight loss of cohoused Piezo2$^{fl/fl}$ ($n = 18$) and Piezo2$^{fl/fl}$Hand2^{cre} ($n = 10$) mice. Mice were administered 2.5% DSS in their drinking water for 8 days. Data are expressed as mean ± SE.
(AE) Summary data of fecal LCN2 production measured via ELISA from Piezo2$^{fl/fl}$ and Piezo2$^{fl/fl}$Hand2^{cre} cohoused mice post DSS administration. ns, no significant difference, two-tailed Student's t test.
(AF) Summary data of fecal LCN2 production measured via ELISA from Piezo1$^{AAV\text{-}GFP}$ and Piezo1$^{AAV\text{-}GFP\text{-}cre}$ cohoused mice post DSS administration. *$p < 0.05$, two-tailed Student's t test.
(AG) Summary data of fecal LCN2 production measured via ELISA from WT and Piezo1^{flpo}ChAT^{cre}Gi cohoused mice post DSS administration. **$p < 0.01$, two-tailed Student's t test.